NASA Contractor Report 172586

INVESTIGATION OF THE "VORTEX TAB"

Keith D. Hoffler

NORTH CAROLINA STATE UNIVERSITY
Raleigh, North Carolina

Cooperative Agreement NCC1-46
May 1985

NASA
National Aeronautics and
Space Administration
Langley Research Center
Hampton, Virginia 23665

ABSTRACT

An investigation was made into the drag reduction capability of vortex tabs on delta wing vortex flaps. The vortex tab is an up-deflected leading edge portion of the vortex flap. Tab deflection augments vortex suction on the flap, thus improving its thrust, but the tab itself is drag producing. Whether a net improvement in the drag reduction can be obtained with vortex tabs, in comparison with plane vortex flaps of the same total area, was the objective of this investigation. Wind tunnel tests were conducted on two models, and analytical studies were performed on one of them using a free vortex sheet theory.

The first test was performed on a 65 deg. delta semi-span model with integral conical flap and tab. In this test, upper-surface pressure surveys and flow visualization studies were carried out. The second test consisted of force and upper-surface pressure measurements on a 74 deg. delta wing/body configuration, having constant-chord flaps to which vortex tabs of varied geometry were added. The analytical portion of this investigation employed the Boeing Free Vortex Sheet code to model the 65 deg. delta. Modifications were made to the code to improve its convergence rate.

The vortex tab at relatively small deflection angles improved the lift-to-drag ratio, but reduced it as tab deflection was increased. Tab planform modifications and area reductions were found to improve the lift-to-drag ratio at high vortex flap deflection angles. The free vortex sheet code predicted the correct trends with flap and tab deflections, in both upper surface pressure and vortex core location changes.

The vortex tab was shown to improve lift-to-drag ratio at high lift coefficients. However, it is unclear from this study whether the improvements would outweigh the increased mechanical complexity of the vortex tab.

LIST OF SYMBOLS

C_A	- Configuration Axial Force Coefficient
C_d	- Drag Coefficient at One Cord Station Derived From Integration of Upper Surface Pressures
C_l	- Lift Coefficient at One Chord Station Derived From Integration of Upper Surface Pressures
C_L	- Configuration Lift Coefficient
$C_{l,\beta}$	- Rolling Moment Coefficient Derivative with Respect to Side Slip Angle
C_N	- Configuration Normal Force Coefficient
$C_{n,\beta}$	- Yawing Moment Coefficient Derivative with Respect to Side Slip Angle
C_M	- Pitching Moment Coefficient
C_p	- Upper Surface Pressure Coefficient
$C_{p,min}$	- Suction Peak
C_R	- Root Cord (inches)
L/D	- Lift to Drag Ratio
SSR	- Sum of the Square of the Residuals
t_{max}	- Wing Maximum Thickness (inches)
X	- Cordwise Distance From Apex (inches)
Y	- Spanwise Distance From Wing Root (inches)
α	- Angle of Attack (degrees)
δ	- Flap or Tab Deflection Angle Measured Perpendicular to Hinge Line (degrees)
η	- Spanwise Distance Measured From Wing Root Nondimensionalized by Local Semispan
Λ	- Sweep Angle (degrees)

SUBSCRIPTS

HL	- Hinge Line
F	- Flap
LE	- Leading Edge
max	- Maximum
T	- Tab

INTRODUCTION

The highly swept wings of typical supersonic tactical aircraft exhibit leading edge separation at moderate to high angles of attack with the corresponding formation of upper surface vorticies (fig. 1). Leading edge separation results in loss of aerodynamic thrust (the attached-flow leading edge suction), which is reflected in a substantial drag increase. Consequent to leading edge separation and vortex rollup, the suction (aerodynamic thrust) is relocated in the vortex core (Polhamus, leading-edge suction analogy, ref. 1). The vortex flap is a down-deflected leading edge portion of the wing which offers forward-facing area on which the vortex suction can act (fig. 1), thus regaining a portion of the aerodynamic thrust. However, down deflection of the vortex flap also reduces the effective leading edge angle of attack, and therefore the strength of the vortex. Deflecting the extreme leading edge portion of the vortex flap (i.e. the tab) upward increases the effective angle of attack, thus augmenting the flap vortex suction (i.e. thrust). At the same time, however, tab deflection reduces the flap frontal area and produces drag itself. In view of these opposing effects, it is not obvious whether the net effect of the vortex tab will be to improve or degrade performance of the plane vortex flap.

In recent studies (ref. 2) the vortex flap has demonstrated considerable potential for improving the subsonic-transonic maneuverability of supersonic tactical aircraft. Several variants of the vortex flap concept have been considered for enhancing its aerodynamic thrust efficiency over an extended range of lift coefficients. One such

variant, heretofore mentioned, is the vortex tab (ref. 3), which is an up deflected leading edge portion of the vortex flap.

Although early flow visualization studies of the vortex tab (ref. 4) confirmed its vortex enhancement capability, few force measurements have been published. In particular, the literature lacks a definitive study comparing the tabbed vortex flap with a plane flap of equal area and on the same wing. In a NASA Langley investigation on a cranked arrow planform (ref. 5), the vortex tab was found to perform better than the plane flap with respect to both L/D and lateral stability at high angles of attack; however, the geometry and size of the two types of flaps in that test were significantly different.

For a proper aerodynamic comparison, it was felt that the total flap area (inclusive of the tab) should be maintained constant within the same basic wing planform. In other words, the deflected tab should be assessed in comparison with the same tab used as a planar extension of the flap surface (plane flap). This was a key consideration in planning the present investigation. In addition, details of the vortex-induced suction and flow characteristics were desired to build a basic understanding of the tab effects. Also of interest was to evaluate the capability of the Free Vortex Sheet code (ref. 6) for predicting the tab aerodynamic characteristics. The Free Vortex Sheet code is an inviscid panel method that predicts pressures on wings with leading edge separation (assuming separation point is known) induced vortex rollup. This code was the first tool used to investigate the vortex tab (ref. 2).

The first part of this investigation consisted of upper-surface pressure surveys and helium bubble and oil flow visualization studies performed on a semi-span 65 deg. delta wing. These tests were carried out in North Carolina State University's subsonic wind tunnel. The 65 deg. delta model had a conical vortex flap and tab that were an integral part of the wing planform. This test examined the effects of various combinations of flap down and tab up deflections. Also the 65 deg. delta model was analytically modeled using the Free Vortex Sheet code, in an attempt to assess the code's ability to predict the effects of tab deflection. The second part of the investigation consisted of force and pressure measurements made on a 74 deg. delta wing-body configuration. This test was performed in the NASA Langley 7- by 10-Foot High Speed Tunnel. The 74 deg. delta model had constant chord flaps and tabs. This test investigated tab area reductions and planform modifications. The results of this investigation are presented in a more condensed form in reference 7.

65-DEG. DELTA MODEL TEST

Figure 2 is a drawing of the 65 deg. delta semi-span model. This model was of composite construction, i.e., having a foam core with fiberglass/resin skin. The trailing edge was left blunt for ease of construction. The flap and tab hinge lines were coincident with the 74.05-deg. and 67.93-deg. swept rays, respectively. These geometrical features were intended to promote an essentially conical leeward flow field, which could then be studied at a single instrumented cross-flow plane. There was a minor deviation from conical geometry in the apex region (up to $X/C_R = 0.14$) where the narrow flap and tab were truncated for structural reasons. The model was pressure instrumented across the span at $X/C_R = 0.7$. There were 43 pressure taps extending from the root to $\eta = 0.946$, with notably close spacing across the hinged surfaces. The hinges allowed flap-down and tab-up deflections to be set independently between 0 deg. and 60 deg. Deflection angles were measured perpendicular to their respective hinge lines. Once flap and tab deflections were set, the gaps under the hinges were taped over to cover the gap and prevent flow spillage through the hinge lines.

The angle of attack, referenced to the wing root chord, varied from 0 deg. to 20 deg. For the oil flow and pressure tests, the tunnel velocity was 88 ft/sec corresponding to a Reynolds number of 0.87×10^6 based on the mean aerodynamic chord. The velocity for the helium bubble experiments was approximately 20 ft/sec.

Test Facility, Instruments, and Methods

The tests were performed in the North Carolina State University Merrill Subsonic Wind Tunnel which is a closed return facility. It has a velocity range from 0 to 100 mph and a turbulence factor of 1.2. The test section, which is 45 inches wide, 32 inches high, and 46 inches long, has plexiglass walls and top and is vented to room pressure. A boundary layer by-pass plate, which represented the plane of symmetry for the semi-span model, was mounted 7.75 inches above the tunnel floor.

Pressure surveys were conducted employing a transducer with a 48-channel scanner which measured the model upper surface static presures with reference to the test section static pressure. The transducer output voltages (± 0.005 mV = ± 0.0003 psi accuracy) were recorded by hand. The pressure data were reduced to coefficient form using software written for a VAX-11/750 system. The pressure distributions were also integrated (via the trapazoidal rule) to obtain the local normal force coefficients, separately across the wing, flap, and tab surfaces. The integrated data were then transfered to NASA Langley's Cyber-173 for further manipulation into lift and drag coefficients.

Oil flow and helium bubble flow visualization methods were used. Thirty-weight motor oil whitened with titanic oxide (TiO_2) was sprayed on the model with the tunnel running at 88 ft/sec. After a satisfactory flow pattern emerged, a photograph was taken of the model upper surface with the tunnel still running. This technique greatly reduced the oil pattern distortion due to gravity effects on the vertically mounted model.

The helium bubble tests were performed using a Sage Action, Inc. Model 3 Bubble Generator in conjunction with an arc lamp and a pair of mirrors. The arc lamp and mirrors were adjusted to illuminate the desired regions of the flow. Bubbles were injected into the flow far enough upstream of the model to allow them to follow natural streamlines to the models leading edge and be entrained into its vortex. Photographs were taken with sufficient exposure time to obtain bubble streaks revealing the streamlines of the flow. The model, boundary layer plate, and mirror set up are shown in figure 3.

Investigation of Model Geometry Effects

Initial tests were performed to check the aerodynamic effects, if any, of the model's blunt trailing edge. Also, the effect of flap and tab truncation in the apex region was investigated.

Figure 4 shows oil flow photographs comparing the patterns before and after the flap and tab were cut and the pressure taps installed. The oil pattern remains essentially unchanged after the modification; specifically, the secondary sepration line moved less than 0.7% of the local span at the instrumented chord station. The most notable variation occurred locally in the apex region where the flap and tab were truncated. Notice the merging of a distinct apex vortex with the vortex emanating from the tab. In some cases (usually with flap deflection and at low α's) the apex vortex remained independent and trailed chordwise over the wing. This produced a minor suction peak in the spanwise pressure distribution. The vortex flow features remain undistorted at

the trailing edge, indicating that the blunt trailing edge of this model was not a source of disturbance to the generally conical nature of the flow field.

Helium bubble studies showed vortex breakdown to cross the trailing edge at α = 18 deg. In ref. 8, this condition occurred at α = 18.5 deg. on a thin full-span planar 65 deg. delta wing, also at low speed. Vortex breakdown is generally considered as the point at which the vortex core becomes unstable. In the helium bubble studies, breakdown was interpreted as the point where the core was no longer well defined.

Shown in figure 5 is a typical upper surface pressure distribution on the planar wing at α = 16 deg. This is quite typical of delta wings, with a relatively low suction level inboard, a local suction peak outboard under the primary vortex, and a secondary separation closer to the leading edge. In view of the high resolution of the pressure distributions obtained with this model, henceforth the individual data points will be dropped in favor of fitted curves, in order to clarify the comparison plots containing several data sets.

Discussion of Results

Typical pressure distribution comparisons between the planar wing (δ_F = 0 deg., δ_T = 0 deg.), the plane flap (δ_T = 0 deg.), and the tabbed flap ($\delta_F = \delta_T$) are shown in figure 6 for four flap deflections at a constant angle of attack of 16 deg. Plane flap deflection reduced the suction peak below the planar wing level at all flap deflections except δ_F = 20 deg., where the reverse occurred. This discrepency will further be discussed in the Free Vortex Sheet section.

Tab deflection increased the flap suction but reduced the suction level on the wing relative to the planar case, at flap deflections of 20, 30, and 40 degrees. This implies a concurrent improvement in the flap thrust and a reduction in the wing drag. At the same time however, high suctions present on the deflected tab generate a drag component.

With the plane flap deflection of 60 deg. (the limit of this study), a pronounced hinge line flow separation occurs leading to vortex rollup as indicated by a suction peak on the wing (fig. 6). A 60 deg. tab deflection not only totally alleviated the hinge line separation, but produced an even lower suction level on the wing than found in the planar case. It also restored the flap suction level almost to that attained on the planar wing at the same angle of attack.

Oil flow photographs of the 60 deg. plane flap and tabbed flap at α = 16 deg. are shown in figure 7. The oil patterns on the wing in the plane flap case show clearly the flap hinge line separation and vortex rollup on the wing. The existence of a small leading edge vortex on the flap and the inboard flow toward the flap hinge line from the primary reattachment line are evident. Tab deflection enlarges the vortex such that it covers the whole width of the flap and thus suppresses hinge line separation. This enlarged vortex fills the flap/tab cavity where the oil flow displays two separation lines, one at the tab hinge line and the other outboard on the tab. The flap separation occurs as the thin boundary layer originating at the primary reattachment line is swept outboard towards the tab hinge corner. It is followed by flow attachment on the tab, and then by the usual secondary separation. This

phenomenon also appears in the pressure distributions with a $C_{p,max}$ occurring at the tab hinge line.

Figure 8 shows C_p distributions for the planar wing, plane flap, and tabbed flap at α = 16 and 18 deg. On the plane flap, increasing α produces an increase in suction peak; on the planar wing and with tabbed flap however, the suction peak decreased with increasing α. The latter trend is an indication of vortex breakdown. Also shown are helium bubble photographs confirming vortex breakdown on the planar wing as well as with the tabbed flap. The breakdown is more extensive with the tabbed flap, resulting in a considerably reduced suction peak relative to the planar wing. Also noteworthy is the tightness of the vortex core (ahead of the breakdown) revealed by the helium bubble photographs of the tabbed flap, in comparison with the other cases. This indicates that the vortex on the plane flap is comparatively weak as expected.

The high resolution of C_p distributions (see fig. 5) obtained on the 65 deg. delta model made it possible, by integration to obtain the upper surface contribution to the normal force at the instrumented semi-span station. In the absence of lower-surface data, the upper-surface normal force could still be used to evaluate trends. This assumption was supported by Free Vortex Sheet solutions, which showed the lower-surface pressure distributions to be relatively insensitive to configuration changes. Integrations were then performed across the wing, flap, and tab sections independently. The resulting local normal forces were then resolved to obtain their individual lift and drag contributions.

Individual sectional drag contributions of the wing, flap, and tab for the 40 deg. flap case are shown in figure 9. As a result of hinge line separation due to flap deflection the wing drag increased slightly at low α's. At α's above 15 deg., however, wing drag was reduced substantially from the planar case, due to delayed inward migration of the vortex. Tab deflection reduced the wing drag throughout the α range and particularly at high α's due to the lowered upper-surface suction as a consequence of increased downwash inboard of the tab-augmented vortex.

The deflected flap drag component is characteristically negative (i.e. thrust producing), at α's below 14 deg., i.e. in the range when the flap upper surface slopes downwards relative to the free stream direction. Tab deflection increases the flap thrust below α = 14 deg. and increases the flap drag above that α, both these effects are consistent with the increased suction on the flap.

The drag contribution of the undeflected tab (since it lies planar with the flap with δ_T = 0 deg.) also remains negative at α's below 14 deg. The drag contribution of the deflected tab, however, surpasses its drag contribution in the planar wing configuration.

In order to assess the overall effect of flap and tab deflections, the sectional configuration drag as a function of α is shown in figure 10. Plane flap deflection reduces the total drag throughout the α range as expected. With the tab also deflected, however, drag is greater than the plane flap case at all α's. Thus, the tab drag contribution is the predominant adverse factor. On the other hand, tab deflection orients its normal force more towards the lift direction, therefore it remains

of interest to examine the L/D characteristics. Figure 11 shows that the L/D with tab deflection is less than that of the plane flap. This implies that the lift increment due to tab deflection was insufficient to overcome its drag increase.

Tab load being a detrimental feature of the tabbed flap configuration, it was thought that a smaller tab deflection (i.e. $\delta_T < \delta_F$) might prove more advantageous. Figure 12 shows the effect of tab deflection on each component as well as the sectional configuration lift and drag at α = 10 deg., with flap deflection held constant at 40 deg. The wing lift decreases slightly with increasing tab deflection, whereas both the flap and tab lift increase. The total configuration lift increases almost linearly with tab deflection. The wing and flap drag decrease slowly with increasing tab deflection; the tab drag, on the other hand, increases rapidly. The sectional configuration drag is found to be a minimum at δ_T = 5 deg. which was the smallest tab deflection tested. At this tab deflection the balance between wing, flap, and tab drag increments appeared optimum for the 40 deg. flap case.

The lift to drag ratio as a function of tab deflection is shown in figure 13. The maximum L/D occurred at δ_T = 5 deg. Higher tab deflections produced successive reductions in L/D. Past δ_T = 25 deg., the L/D fell below the undeflected tab case with α = 10 deg. This crossover occurred at lower tab deflection angles as α was raised, except at α = 20 deg. where the trend reversed. This reversal was probably due to the inability of the tab to further augment an already strong vortex, especially close to its breakdown.

Conclusions

Increasing tab deflection augments vortex suction on the flap as well as its own upper surface. Although the flap frontal area is reduced, lift producing area is increased with tab deflection. The stronger downwash induced on the wing by the tab augmented vortex reduced wing suction and therefore its drag. The net effect of large tab deflections ($\delta_T = \delta_F$) was to decrease L/D. However, with smaller tab deflections ($\delta_T < \delta_F$), L/D improvements were realized.

74 DEG. DELTA TEST

An existing NASA Langley 74 deg. delta wing-body configuration model, whose principal dimensions are shown in figure 14, was fitted with vortex tabs for this test. Spanwise pressure distributions were obtained on the wing and flap surfaces at five stations as indicated; the tabs however, were not pressure instrumented.

Vortex tabs were fabricated from 1/16-inch thick aluminum sheets and bolted to the lower surface of the constant-chord flaps. The tabs were initially tested at 0 deg. deflection (i.e. as planar extensions of the flaps) to establish the baseline case, followed by tests of tab-deflected configurations. Tab planform modifications and area reductions were also investigated. The various tab planform shapes and their corresponding areas are shown in figure 15.

Two test series were run, both at Mach 0.3 and a Reynolds number of 5.2×10^6 based on the mean aerodynamic chord. The first test obtained longitudinal force data and upper surface pressure distributions through an angle of attack range from 0 to 20 deg. The vertical tail was not present in this test. In the second test entry, with the vertical tail installed, longitudinal force data and lateral directional derivatives were measured. The α range for this test was 0 to 20 deg. with sideslip angles of 0 deg., and ± 5 deg.

Facility

The tests were performed in the NASA Langley 7- by 10-Foot High-Speed Tunnel which is a continuous flow closed return subsonic-transonic atmospheric facility (ref. 9). The first test obtained longitudinal force data and upper surface pressures with the model supported on the standard angle of attack sting, which has an angle-of-attack range of 24 degrees.

The second test obtained longitudinal force data and lateral directional derivatives, with the model supported on the high angle static stability sting. This sting has a computerized controller and provides a pitch capability of -10 deg. to 60 deg. and a roll capability of -180 deg. to 180 deg. Combinations of pitch and roll were used to obtain the desired angle of attack and sideslip.

Comparison of data between the two tests indicated some discrepancies. Although the trends matched well, the axial force results did not repeat, even after the the vertical tail drag increment was accounted for. The different stings used in the two tests appeared to produce different levels of aerodynamic interference at the model. The high-angle sting was considerably bulkier than the standard alpha sting, a factor not taken into account in the blockage corrections. Blockage corrections for the model were made using reference 10, and jet boundary corrections were made using reference 11.

Both tests used a six component strain gauge balance to measure force data. Pressure data in the first entry were measured using two 48 port scanning valves.

The facility's data acquisition, display, and control system consists of a Honeywell (Xerox) Sigma 3 computer, an external input/output processor, 4.5 megabytes of rapid access disk storage, two nine-track tape drives, a card reader, a line printer, a Tektronix 4014 graphics terminal and hard copy unit, a data aquisition unit, and a data link to Langley's central computing complex. For detailed information on this data aquisition system see reference 12.

Discussion of Results

Baseline Tab: Tests on this model concentrated on cases with tab deflection set equal to the flap deflection. Although this may seem unduly restrictive, it formed a convenient basis for evaluating the tab modification effects.

Figure 16 shows a typical pressure distribution for the planar wing, a plane flap deflection, and a tabbed flap deflection at the 74% chord station. The general trends here correspond well with those seen in the 65 deg. delta test. With flap deflection the wing suction decreases, and the suction peak on the the flap increases while the vortex "footprint" narrows. These effects are further accentuated with tab deflection.

Figure 17 shows L/D as a function of C_L for 15 deg. plane flap deflection and the same flap deflection with positive (up) as well as negative (down) tab deflections. This comparison was included as a further test of the relative importance of flap suction versus frontal area to the overall L/D characteristics. At $C_L < 0.4$, negative tab

deflection produced an L/D improvement over the plane flap, whereas the opposite occurred with the positive tab deflection. The largest effects occurred near L/D_{max}; above C_L of 0.4 there was no significant change in L/D with either tab deflection. Shown in figure 18 are upper surface pressure distributions corresponding to $C_L = 0.5$ for the flap deflected cases. An up tab increased the flap suction and reduced the wing suction, whereas the down tab produced the reverse effect.

Since increased flap suction and reduced wing suction are both positive factors for drag reduction, the higher L/D obtained in the tab-down deflection case points to the importance of frontal area. In addition, tab drag is eliminated and most probably replaced by a thrust contribution. While the tab-down case is favorable to L/D_{max}, it does not appear to be useful for improving L/D at higher lift coefficients. It was reasoned that at higher flap deflections (increasing tab deflection on the highly deflected flap would eventually result in the formation of a vortex under the flap and tab) which produce greater frontal area, tab-up deflection to augment the flap suction may be a better option, particularly in order to improve L/D at higher lift coefficients therefore, in the further tests at 30 deg. and 45 deg. flap deflections only tab-up deflections were considered.

Upward tab deflection affects the overall configuration thrust through a combination of (1) augmented vortex suction on the flap, (2) reduced flap frontal area, and (3) direct drag of the tab. The net change in the thrust can best be seen in the axial force component. The coefficient of axial force vs. normal force are plotted in figure 19.

At constant angles of attack the normal force increased with tab deflection in both cases, as expected. However, the corresponding axial force increments were opposite ($\alpha < 16$ deg.): on the 30 deg. flap, tab deflection reduced flap thrust ($-C_A$), but increases it at $\delta_F = 45$ deg. Above $\alpha = 16$ deg. tab deflection reduced flap thrust ($-C_A$) for both flap deflections. L/D vs. C_L for the above flap/tab combinations are shown in figure 20. Tab deflection is adverse to L/D with $\delta_F = 30$ deg., but is beneficial at $\delta_F = 45$ deg. These opposite effects are in tune with the respective axial force increments of the previous figure.

The reason for these opposite trends may be found in spanwise pressure distributions across the wing and flap (but excluding the uninstrumented tab) at $x/C_R = 0.74$ and $\alpha = 16$ deg., shown in figure 21. The flap suction increment with tab deflection was much greater on the 45 deg. flap. The improvement in the 30-deg. flap suction was not sufficient to overcome the loss in frontal area (as seen in axial force plots) whereas, on the 45 deg. flap the increased flap suction did overcome the loss in frontal area. Also seen in the pressure distributions for $\delta_F = 45$ deg. is the significant reduction of wing suction which is a primary source of drag. This improvement is attributed to suppression of hinge line separation in the 45 deg. flap case, which is a direct result of the increased downwash on the wing produced by the augmented vortex. These examples indicate that the tab is more beneficial at high flap deflections.

Tab Modifications: Although the tab on this model was not instrumented, reference to the 65-deg. delta results indicates that the tab

load constitutes a substantial portion of the configuration drag. Therefore, preliminary attempts were made to reduce the tab planform area both by limiting its span and through planform shaping. Since cutting the tabs was irreversible, separate routes were taken on the 30 deg. and 45 deg. tab. The baseline (full-span one inch chord) 45 deg. tab was first bisected spanwise to generate a 1/2 inch chord full-span tab, and then bisected chordwise producing a fore and aft segment. The baseline 30 deg. tab was first notched at half the extent of its chord, then it was cut through chordwise, forming separate fore and aft constant-chord segments. The constant-chord segments were then shaped into inverse taper (or delta) tabs. The part-span tabs were tested individually in both the fore and aft positions on the flap. Sketches of all the test configurations are shown in figure 15.

The L/D results of the tab planform modifications are summarized in the bar chart of figure 22. The shaded areas represent L/D increments over the planar wing at L/D_{max} and at $C_L = 0.5$.

On the 30 deg. flap, going from plane flap to a 30 deg. baseline tab case reduces L/D_{max}. Tab modifications viz. notched tab, delta segmented tabs, and both inboard tab segments all lead to further L/D_{max} reductions. With only the aft tab segments on however, the L/D_{max} recovers to a level marginally above the 30 deg. baseline tab. However, even the best tab modification does not match the 30 deg. plane flap L/D_{max} which remained the best of all cases tested. As for L/D at $C_L = .5$, the aft constant chord segment tab was the best, with the aft delta and the 30 deg. baseline tab coming second and third.

In the 45 deg. flap case only one planform modification is shown. As seen before, the 45 deg. baseline tab improved both the L/D_{max} and L/D at C_L = .5 over the plane flap deflection. The half-span aft constant-chord tab produced virtually the same L/D's as the baseline tab, indicating that narrow tabs in a proper part-span position are the most efficient.

Figure 23 shows the pressure distribution across the flap and wing at four chord stations at α = 16 deg. (C_L = 0.5). This figure helps to explain the L/D improvement produced by the aft constant-chord tab over the baseline case. At the forward stations the vortex suction was distributed across the flap and the drag-producing baseline tab. With the forward segment of the tab removed, not only was its drag eliminated, but the flap suction (i.e. thrust) was increased. At the aft stations the flap suction peaks were reduced slightly, but the vortex migration to the wing was still prevented. The 45 deg. flap case was generally similar, except that the inward migration of the vortex was reduced in the forward region and the suction peak reductions over the aft region were greater. These effects apparently offset each other.

The part-span aft tab has shown promise in these investigations, and undoubtedly further modifications could show further improvement.

Longitudinal Stability: Longitudinal stability of the planar wing, 30 deg. plane flap, 30 deg. tabbed flap, and 30 deg. flap with 30 deg. aft delta tab are shown in figure 24. The moment reference used resulted in a relatively high static margin for a typical aircraft of this type. The results however, are used only for comparisons of the

configurations tested. The planar wing shows a pitch up at α 14 deg. Vortex flap deflection eliminated the pitch-up and produced a more stable configuration. Tab deflection caused even greater stability at the higher α's. The use of aft inverse-tapered tabs caused a strong nose down pitching moment. The nose down pitching moment could be helpful in recovery from a high angle of attack maneuver.

Lateral Stability: The lateral stability results were produced from the second tunnel entry. For this entry the baseline tabs (already modified) were not available. Results here are presented for the planar wing (without the 0 deg. tab area extension), the 30 deg. plane flap (without the 0 deg. tab), and the 30 deg. flap with the 30 deg. aft inverse taper tab. Note, in these tests the vertical tail was on.

The top portion of figure 25 shows the stability in roll of the three configurations. The planar wing is more stable in roll than the flap and flap/tab deflected cases.

The bottom of figure 25 shows the yawing stability of the three configurations. The planar wing becomes unstable at α = 16 deg. The plane flap and tabbed flap configurations become unstable at α's of approximately 11 deg. and 12 deg., respectively.

Flap and flap/tab deflections have a destabilizing effect in both roll and yaw. In roll, even though stability is reduced none of the three configurations goes unstable. The yawing stability limit is reduced about 5 deg. in α by the 30 deg. flap deflection and 30 deg. aft inverse taper tab configuration.

Conclusions

The trends with tab deflection were generally in good agreement with the 65 deg. delta test. High tab deflections (i.e. $\delta_F = \delta_T$) appear to be capable of improving L/D at high flap deflections (δ_F = 45 deg.). At lower flap deflections tab planform modifications were shown to improve the L/D over the plane flap at high C_L, but to reduce the L/D_{max}.

FREE VORTEX SHEET COMPUTATIONS

The Free Vortex Sheet (FVS) theory (ref. 6) has been used with considerable success to predict the aerodynamic characteristics of highly swept configurations. The theory is fully three dimensional and predicts with good accuracy wing surface pressures and hence, forces and moments. It also predicts the vortex shape and core location. The theory neglects viscosity and assumes the leading edge to be the location of separation. This study primarily sought to validate the codes capability to predict trends with flap and tab deflections.

Convergence Properties

Achieving convergence with the FVS code, while relatively easy for planar wings, has proven more difficult with vortex control devices such as the vortex flap and was not possible with conical starting solutions. This problem was alleviated to some extent by development of the "partial restart" procedure (ref. 13), which employs free and fed sheet geometries from previous computations as starting solutions for new computations. Although successfully applied on a variety of configurations (refs. 13 and 14), in vortex flap applications the method has been limited to small increments in δ_F and α. With the "partial restart" procedure and some user-manipulation of the starting vortex shape, convergence has been obtained for more difficult cases (ref. 15).

During the course of this investigation, modifications were made to the FVS code to allow the user to easily and systematically rotate and/or radially scale the entire, or any column of the free and fed

sheets about the leading edge (see Appendix A). This modification (modified partial restart) provided convergence for the flap-deflected cases with considerably less user and CPU time than would otherwise have been required.

Convergence with deflected tab configurations was very fast with the "partial restart" procedure using sheet shapes from the plane flap case.

Numerical Model

Shown in figure 26 is the conical model and its paneling, chosen to validate FVS solutions against experimental results from the 65 deg. delta wing. The computational model deviated from the wind tunnel model in assuming zero thickness and not truncating the flap and tab. These presumably minor differences were accommodated in order to simplify the modeling and promote convergence. Continuing the flap and tab to the apex eliminated the leading edge discontinuity, thus allowing the free and fed sheets to originate at the apex. A spanwise row of control points was located at $X/C_R = 0.7$ for direct comparison of upper surface pressures between FVS and experiment.

Discussion of Results

Comparisons between theoretical and experimental core locations for three cases, viz. the planar wing, the maximum plane flap deflection, and corresponding flap/tab deflection case, are shown in figure 27. The core moved outboard and closer to the flap surface as the flap was

deflected downward; at a constant δ_F, tab deflection then moved the core back inboard and upward from the flap surface. Trends in vortex core movement were predicted well by FVS. The codes ability to predict exact core locations improved with flap and flap/tab deflections over the planar wing.

Theoretical and experimental C_p distribution comparisons for all configurations tested are shown in figure 28. In all cases, vortex-induced suction was overpredicted by the free vortex sheet code. This is typical free vortex sheet behavior. Some possible reasons for the discrepancy between theory and experiment are: (1) model geometry (which includes experimental model wing thickness and flap/tab truncation in apex region); (2) tunnel flow inclination and wall interference for which no corrections were made; and (3) the primary reason, viscous effects, especially secondary separation.

A concise assessment of the FVS capability for predicting overall trends is presented in figure 29. The top part of this figure shows the variation of suction peak ($C_{p,min}$) vs. plane flap deflection. Initially flap deflection (i.e. to δ_F = 20 deg.) raises the suction peak above the planar-wing level as the vortex core is pulled closer to the flap. A further increase in δ_F to 30 deg., however, reduces the suction. Here the reduction in vortex strength apparently overrides the effect on the vortex-core proximity to the flap surface. This trend with flap deflection is further accentuated in FVS, presumably because secondary separation (which may have a softening effect on the primary suction peak development) is neglected.

The effect of tab deflection with a constant flap deflection of 30 deg. is shown in the lower part of figure 29. A steady rise in suction peak level with increasing δ_T is shown by FVS as well as experimental data. Since the vortex core is progressively moving away from the flap at the same time, this increase in suction reflects the dominating effect of vortex augmentation due to tab deflection.

Conclusions

Trends in both upper surface pressure distributions and vortex core location are predicted well with flap and tab deflection by the FVS code. The FVS overpredicted suction peaks in each case. Initially, with small flap deflections, flap suction variation is dominated by vortex core movement rather than vortex weakening; with higher flap deflections the reverse is true. Flap suction modification due to tab deflection is primarily determined by vortex strength enhancement and less by the core movement.

CONCLUDING REMARKS

The objective of this investigation was to obtain a preliminary assessment of drag-reduction effectiveness of the vortex tab relative to the plane vortex flap, under the assumptions that the two flap systems are of the same total area and are integral to the basic wing planform. Wind tunnel studies on two delta wing configurations were performed. Upper-surface pressures on a 65 deg. delta wing provided basic trends of sectional lift and drag components with various combinations of flap and tab deflections. Supporting flow visualizations aided in understanding the flow field characteristics responsible for the observed trends. Force measurements (also supported by pressure data) on a 74 deg. delta indicated the overall performance of vortex tabs in comparison with plane flaps on an equal area basis, and provided the opportunity to study the potential of vortex tab planform modifications to improve L/D. The ability of Free Vortex Sheet Theory to predict tab deflection effects on the 65 deg. delta model was also tested.

The results indicate that although the integral tab augments vortex suction on the flap, thus improving flap thrust contribution, direct tab drag more than nullifies that benefit. Attempts to reduce the tab drag through smaller tab deflection as well as through tailored-planform and part-span tabs produced promising results. With tab up deflections considerably less than the flap down deflection a portion of the tab normal force remained thrust-producing while still enhancing the vortex suction on the flap. Part span tabs with the forward portion of the tab removed, reduced the tab drag penalty, while the remaining aft tab

segment enhanced the vortex flap thrust in that region and delayed vortex inboard migration.

The free vortex sheet code predicted the proper trends in both upper-surface pressure distributions and vortex core locations with flap and tab deflections. Quantitatively, however, the code overpredicted suction peaks throughout.

Incidental advantages of the vortex tab include partial recovery of the vortex lift lost by plane flaps which may help reduce the angle of attack at landing, and also the possibility of longitudinal trimming through aft-tab adjustment. It is not conclusive from the limited scope of the present study whether the aerodynamic benefits of the vortex tab out-weigh the added mechanical complexity and weight.

Certain guidelines for improving tab effectiveness can be drawn as follows:

1. Minimize tab area to reduce its drag.
2. Vortex tab is not useful in the forward (or inboard) region of the flap, here the tab area should be reduced or eliminated altogether.
3. Tab planform shaping can improve configuration L/D at higher lift coefficients.
4. Tab deflections less than the flap deflection are beneficial to L/D.

Using these guidelines a tab design to improve configuration L/D and reduce the inherent nose-up pitching moment in subsonic-transonic maneuver of supersonic tactical aircraft should be possible.

RECOMMENDATIONS

Further studies of the vortex tab should investigate the combined effects of reduced tab deflection and area. Also the effect of tab hinge line sweep should be studied. Increasing tab hinge line sweep would increase the tab deflection at which the tab axial force changes from thrust to drag at a given flap deflection; this could make higher tab deflections more beneficial. A possible tool for the design of this next step model might be the NASA Langley Vortex Flap Design method, which might be applicable to vortex flap/tab combinations. The flap and tab designed by this method might resemble the sketch shown in figure 30.

APPENDIX A

Free Vortex Sheet Code Modification

The application of free vortex sheet theory to vortex control concepts has attracted much interest in recent years. Boeing's Free Vortex Sheet computer code (ref. 6) is fully three-dimensional and predicts pressure distributions, and thus forces and moments, on highly swept wings with leading edge separation and vortex rollup. The shape of the leading edge vortex sheet and the core location are also predicted. The code is iterative in nature, convergence being comparatively easy to achieve for planar wings at high α's when the leading edge sweep angle is 60 deg. or greater. Convergence was not possible however with vortex control devices such as vortex flaps, using conical flow starting solutions.

This problem was alleviated to some extent by the development of the "partial restart" procedure (ref. 13). This procedure uses the converged sheet networks from one case as the starting solution for another case. Although this method has been quite successful, it was limited to small increments in δ_F and/or α. With the "partial restart" procedure and some "user-manipulation" of the sheet shapes, convergence has been obtained for more difficult cases (ref. 15). During this investigation an attempt was made to incorporate user-manipulations into the code and make their use easy and systematic. This attempt was quite successful in reducing both user and CPU time, and is briefly described in the following.

The code modification allows the user to rotate and/or radially scale the entire or any column of the free and fed sheets of the starting solution about the leading edge of the configuration. Its basis was the observation that obtaining convergence is less difficult when the sheets are globally contracting towards the solution.

The free and fed sheets from the planar case at $\alpha = 16°$ were attached via the partial restart procedure, to the case with $\delta_F = 15$ deg. and $\alpha = 16$ deg. These sheets were first attached directly, and then employing the rotation/scaling modification (modified partial restart). Convergence was successful only with the modified partial restart. Figure 31 shows that the modified partial restart sheet geometry bounds the converged solution allowing the sheets to globally contract towards convergence; whereas, the standard partial restart did not bound the converged solution. Convergence was also attempted with the sheets only rotated but not expanded. This attempt was not successful because the converged solution was not bounded near the leading edge.

Figure 32 shows the rate of convergence for the $\delta_F = 15$ deg. case using the modified and standard partial restart from the planar wing. Convergence was obtained in seven iterations with the modification. Previously, convergence with the standard partial restart could only be obtained for high flap deflections by stepping down the flap deflection in 5 to 7 deg. increments. This took 4 to 5 iterations per 5 to 7 deg. increment; therefore, the CPU time required to set up at least 1 partial

restart and perform 1 to 3 iterations was saved by the modified partial restart procedure, also user time and effort was greatly reduced.

Figure 33 shows the convergence rate on a 20 deg. flap deflection at α = 16 deg. The sheet geometry used by the standard and modified partial restart routine was taken from the converged solution on the 15 deg. flap deflection. With this 5 deg. increment in flap deflection convergence was obtained in 5 iterations in both cases. This implies that the modified partial restart procedure can be used with confidence in cases where convergence is doubtful.

The convergence rate on a 30 deg. flap configuration with sheet geometries taken from the 20 deg. flap configuration is shown in figure 34. Convergence was obtained only with the modified partial restart for the 10 deg. step in δ_F.

The modification to the code was found to be a useful tool in this investigation. It proved simple to use, with rotations equal to the flap deflection increment, and expansions of 5% to 6% promoting convergence. The modification allowed double the flap deflection increments than previously possible, thus cutting both user and CPU time (flap deflection increments greater than 15 deg. were not attempted). The convergence rate was not affected in cases where the modification was used but not needed. The ability of the modification to promote convergence in other more difficult cases (i.e., gothic leading edges, cambered leading edges, low α's, etc.) seems probable.

REFERENCES

1. Polhamus, E. C., "A Concept of the Vortex Lift of Sharp-Edge Delta Wings Based on a Leading-Edge-Suction Analogy", NASA TN D-3767, 1966.
2. Rao, D. M., "Vortical Flow Management for Improved Configuration Aerodynamics - Recent Experiences", AGARD-CP-342, April 1983.
3. Tinoco, E. N. and Yoshihara, H., "Subcritical Drag Minimization for Highly Swept Wings With Leading Edge Vorticies", AGARD-CP-247, Oct. 1978.
4. Runyan, L. J., Middelton, W. D., and Paulson, J. A., "Wing Tunnel Test Results of New Leading Edge Flap Design for Highly Swept Wings - A Vortex Flap", NASA CP-2108, Part I, pp. 131-147, Nov. 1979.
5. Yip, Long P. and Muri, Daniel G., "Effects of Vortex Flaps on the Low-Speed Aerodynamic Characteristics of an Arrow Wing", NASA TP-1914, 1981.
6. Tinoco, E. N., Lu, P., and Johnson, F. T., "An Improved Panel Method for the Solution of Three-Dimensional Leading-Edge Vortex Flow Volume II - User's Guide and Programmers Document", NASA CR-3279, 1980.
7. Hoffler, Keith D. and Rao, D. M., "An Investigation of the 'Tabbed' Vortex Flap", AIAA-84-2173, Aug. 1984.
8. Wentz, William H., Jr. and Kohlman, David L., "Wind Tunnel Investigations of Vortex Breakdown on Slender Sharp-Edged Wings", NASA CR-98737, Nov. 1968.

9. Fox, C. H., Jr. and Huffman, J. K., "Calibration and Test Capabilities of the Langley 7- by 10- Foot High Speed Tunnel", NASA TN X-74027, 1977.

10. Herriot, J. G., "Blockage Corrections for Three-Dimensional-Flow Closed-Throat Wind Tunnels, with Consideration of the Effect of Compressibility", NACA Rep. 995, 1950.

11. Gillis, C. L., Polhamus, E. C., and Gary, J. L., Jr., "Charts for Determining Jet Boundary Corrections for Complete Models in 7- by 10-Foot Closed Rectangular Wind Tunnels", NACA NR L-123, 1945.

12. Fox, C. H., Jr., "Real Time Data Reduction Capabilities at the Langley 7- by 10-Foot High Speed Tunnel", NASA TM 78801, 1980.

13. Luckring, J. M., Schoonover, W. E., Jr., and Frink, N. T., "Recent Advances in Applying Free Vortex Sheet Theory for the Estimation of Vortex Flow Aerodynamics", AIAA-82-0095, Jan. 1982.

14. Frink, Neal T., "Analytical Study of Vortex Flaps on Highly Swept Delta Wings", ICAS 82-6.7.2, Aug. 1982.

15. Erickson, Gary E., "Application of Free Vortex Sheet Theory to Slender Wings with Leading-Edge Vortex Flaps", AIAA Paper No. 83-183, July 1983.

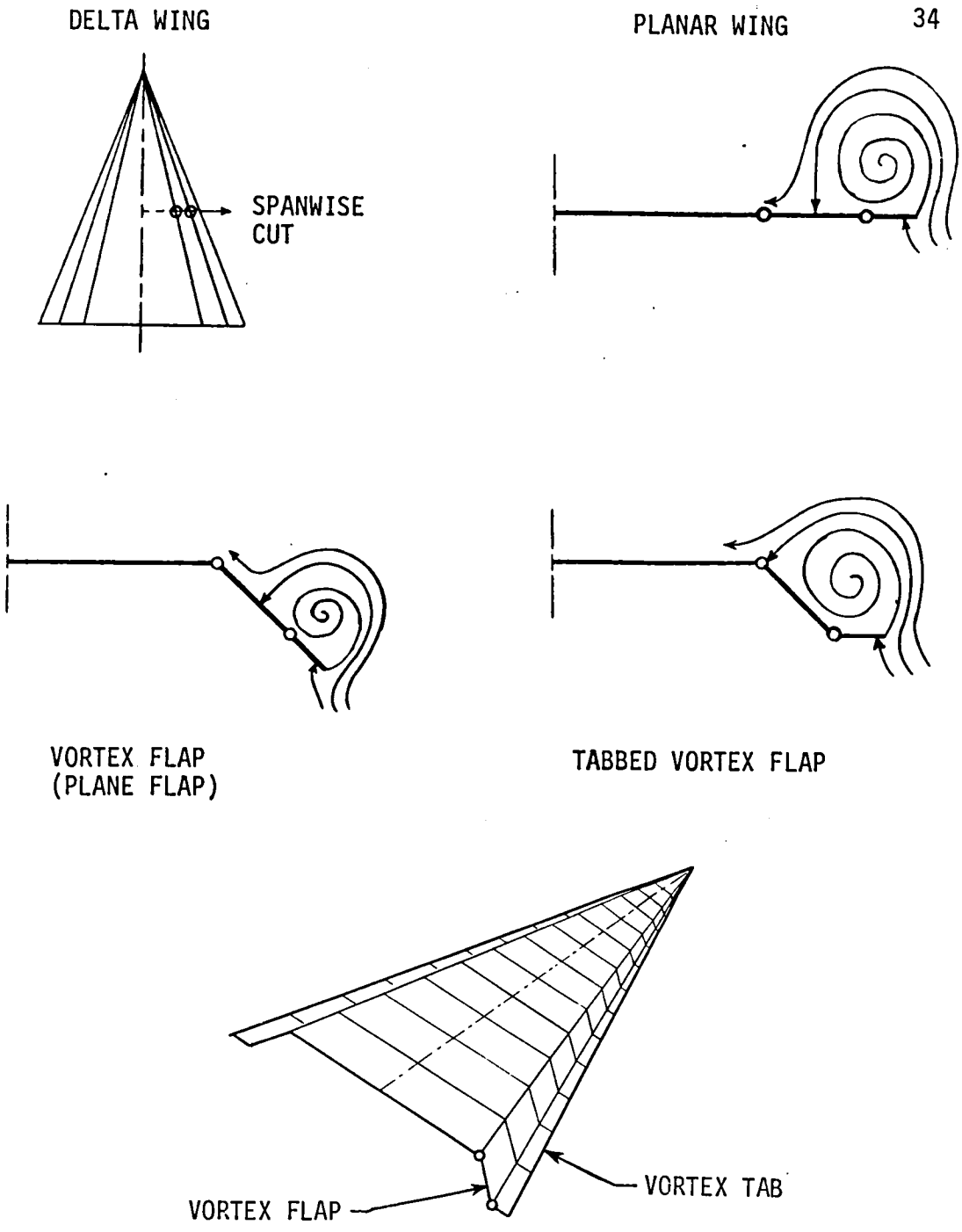

FIG. 1. Tabbed vortex flap concept.

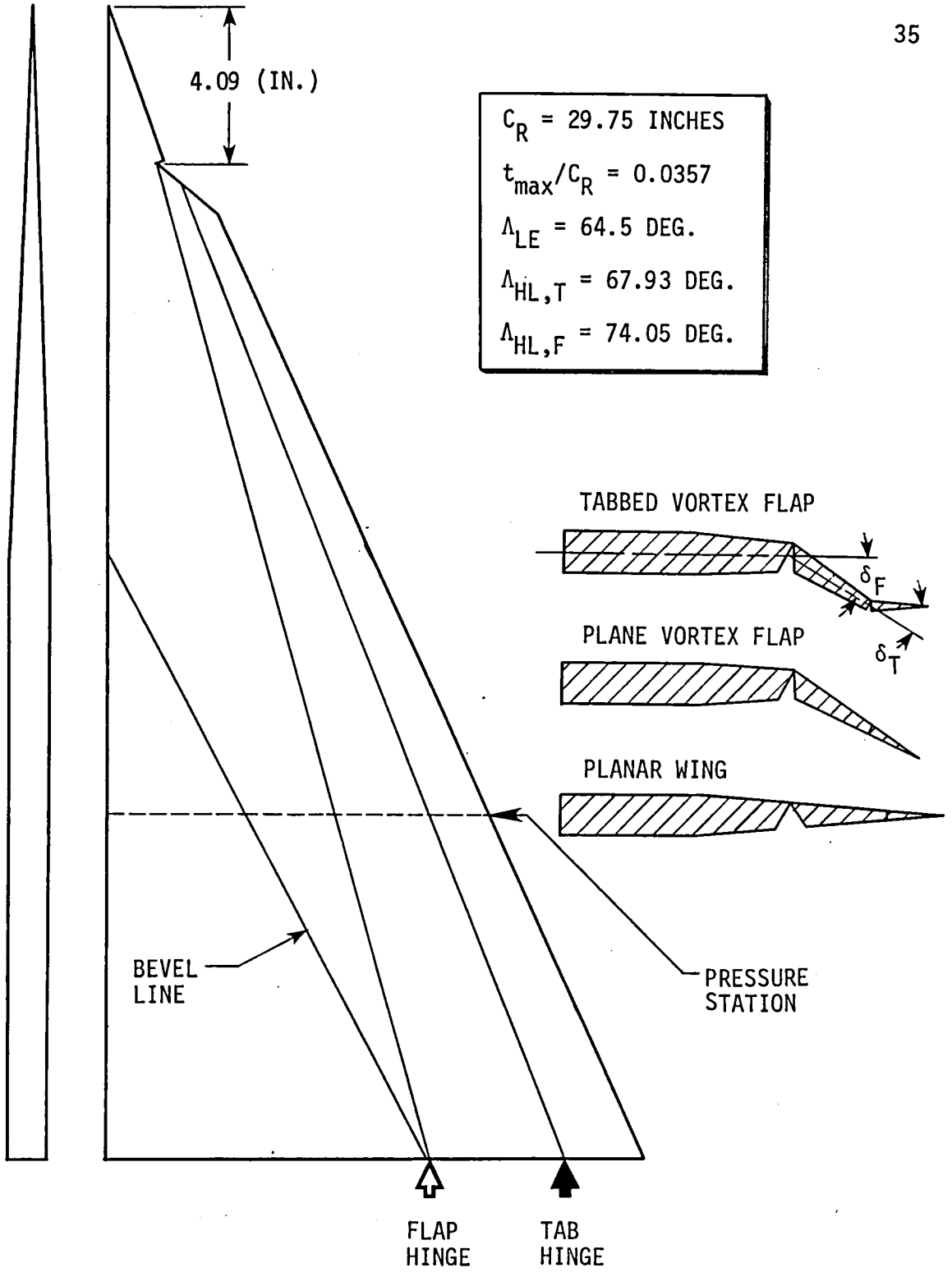

FIG. 2. 65-deg. delta semi-span model with integral "conical" flap and tab.

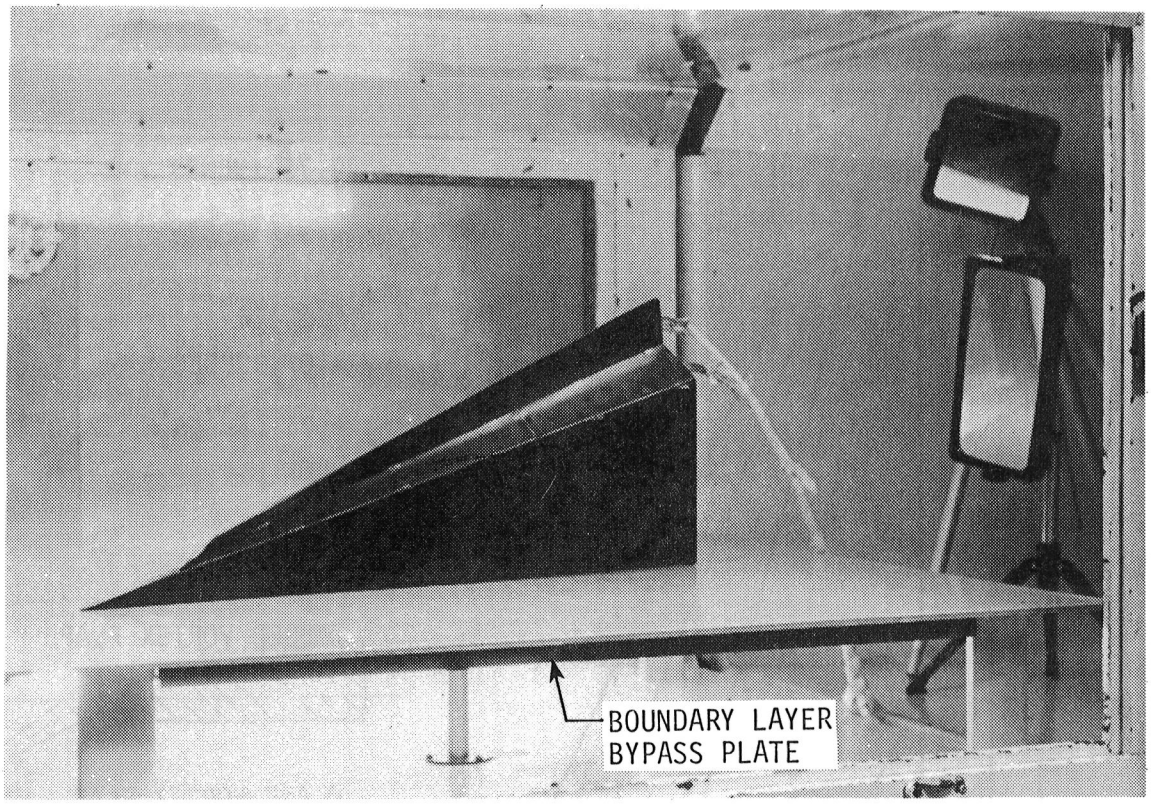

(a) Photograph of model in test section.

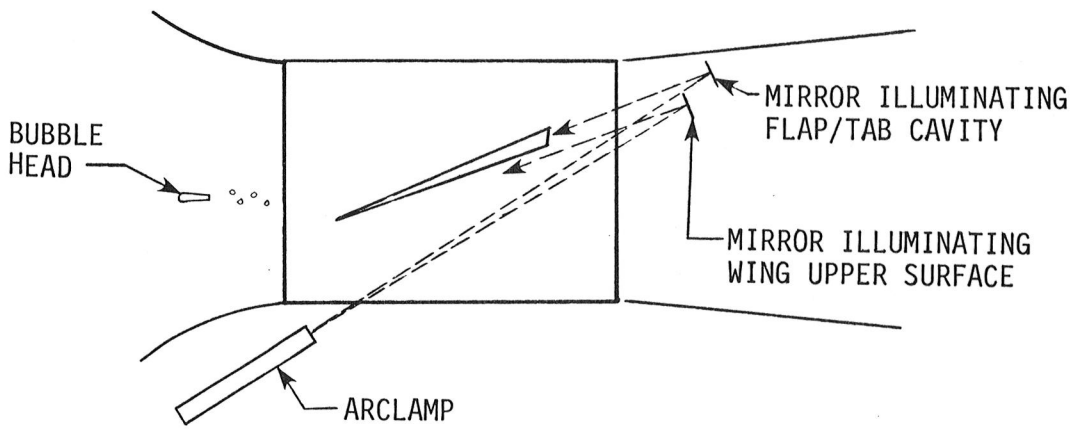

(b) Top view of test section with model and helium bubble setup.

FIG. 3. Model, boundary layer bypass plate, and helium bubble setup for NCSU test.

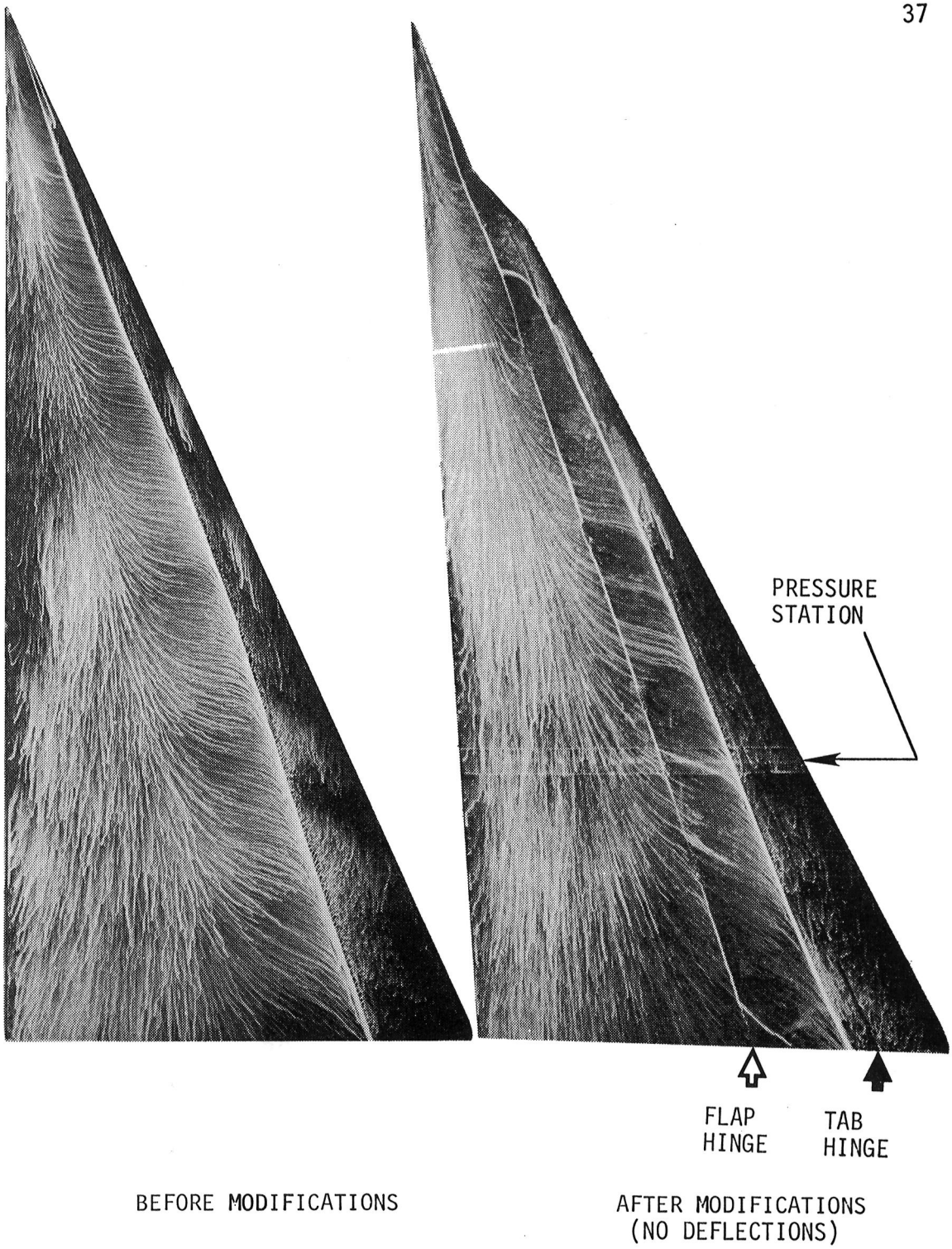

FIG. 4. Upper-surface oil patterns on planar wing at $\alpha = 16^{o}$ before and after the flap and tab were cut and pressure taps were installed.

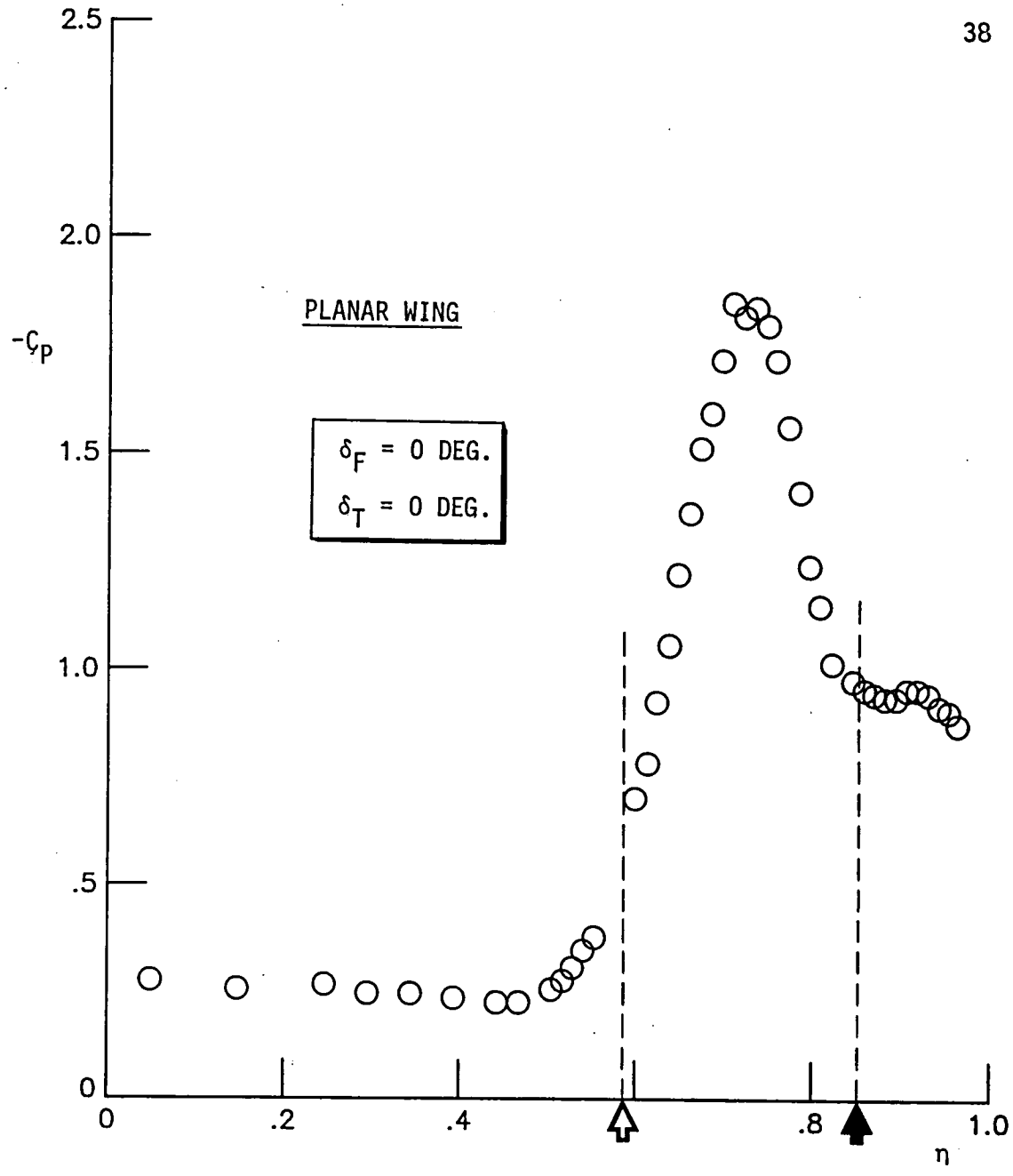

FIG. 5. Pressure distribution on planar wing at $\alpha = 16^o$ and $x/C_R = 0.7$.

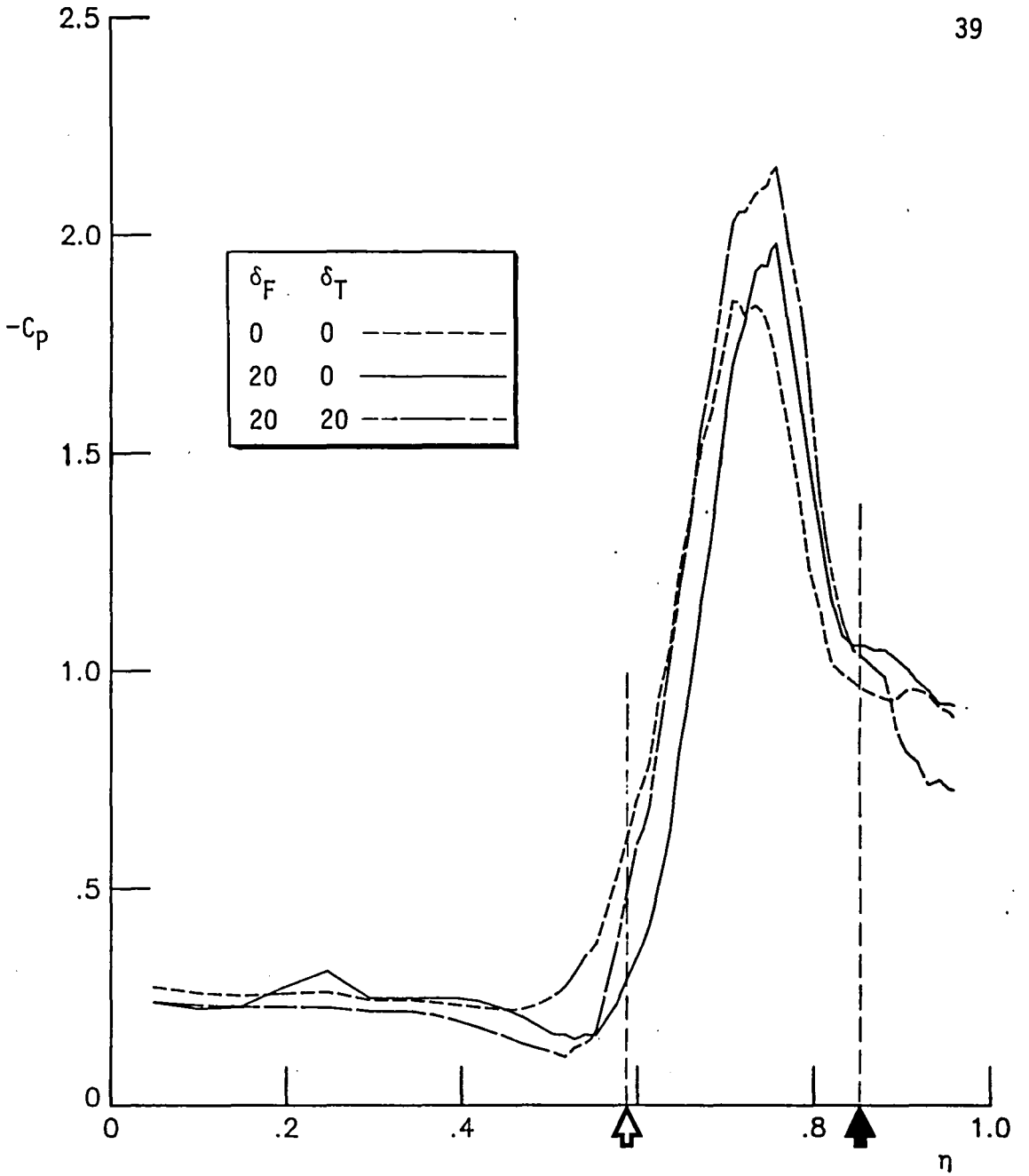

FIG. 6. Flap/tab deflection series at α = 16 deg. and X/C_R = 0.7.

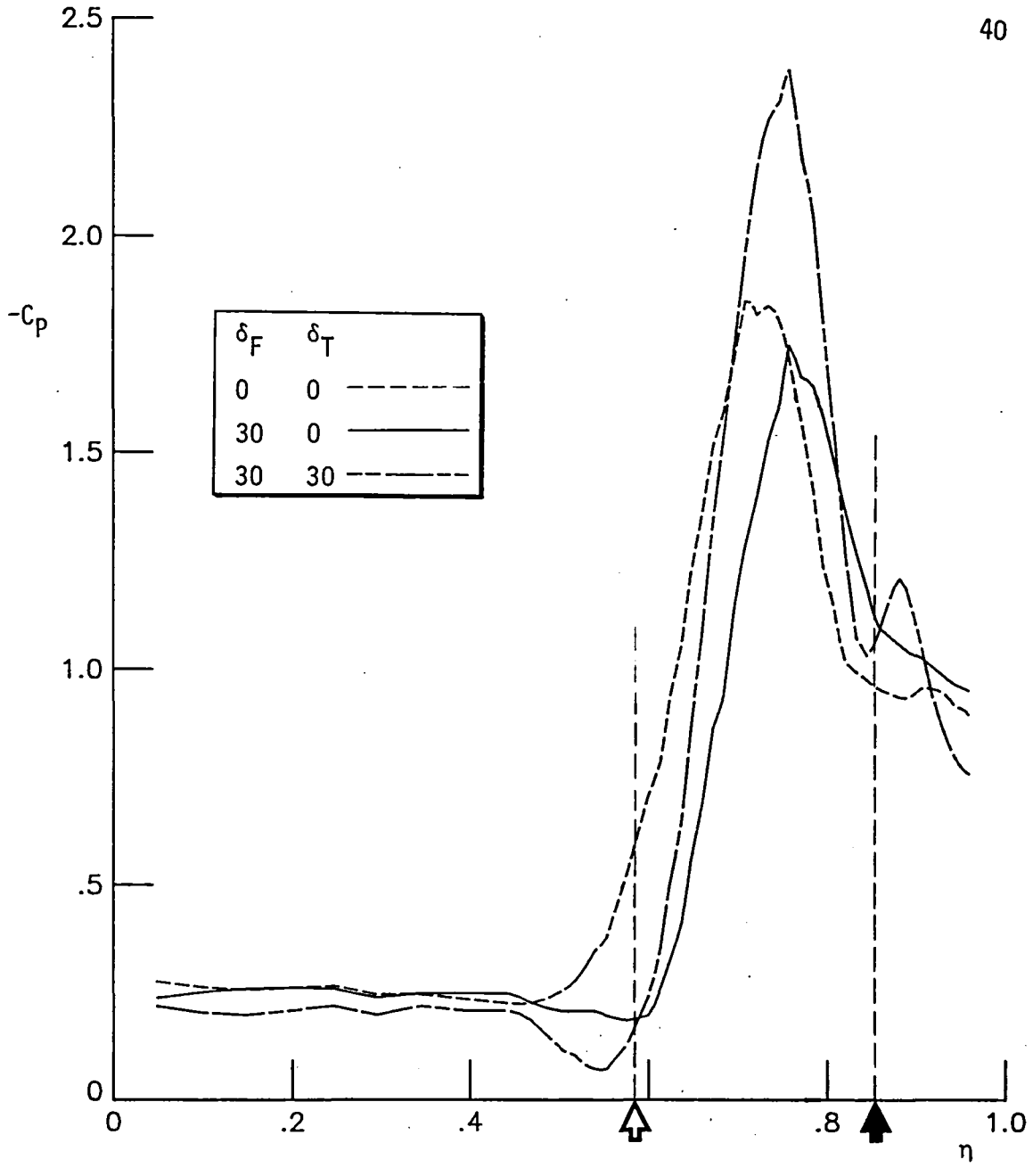

FIG. 6. (continued)

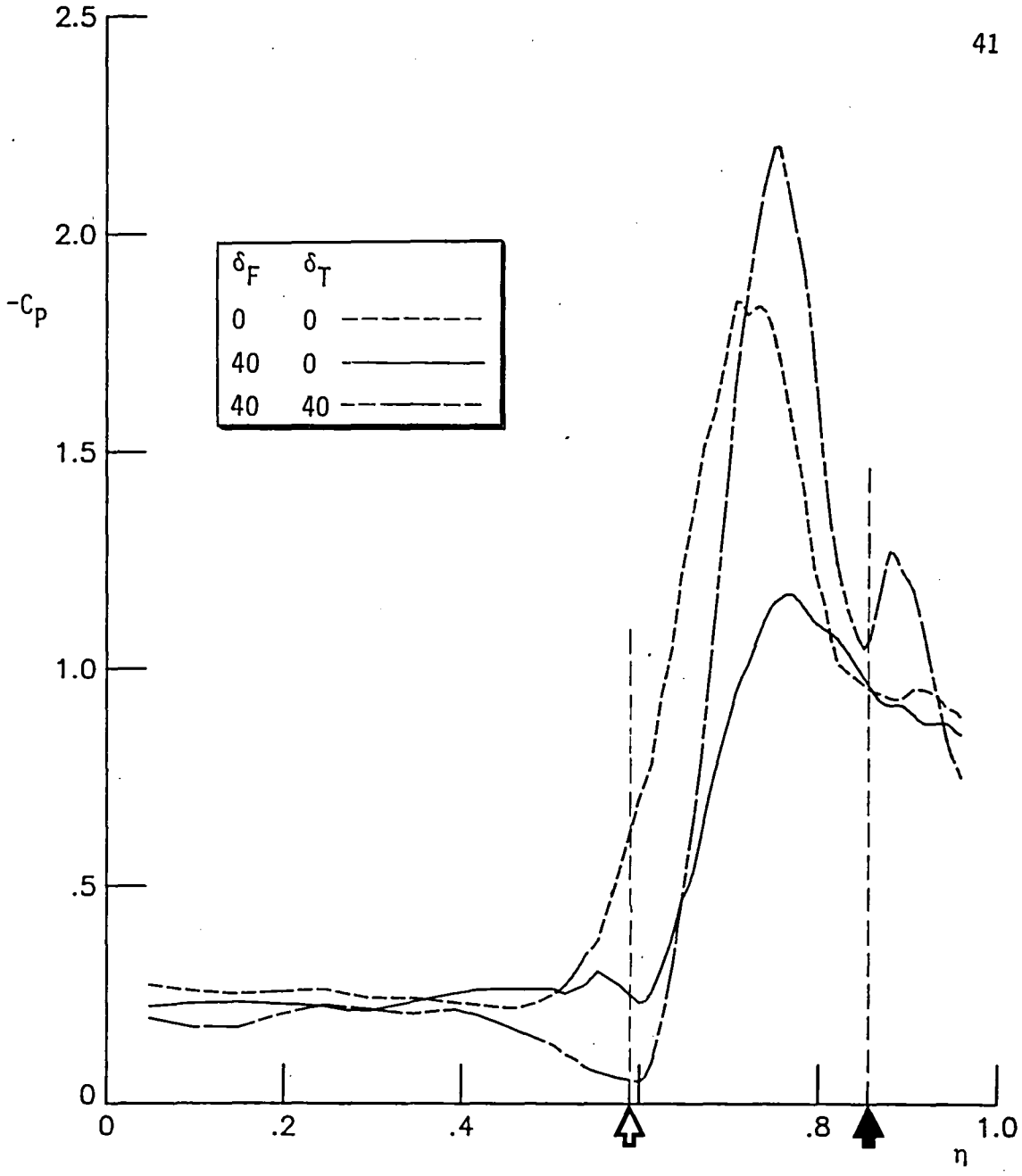

FIG. 6. (continued)

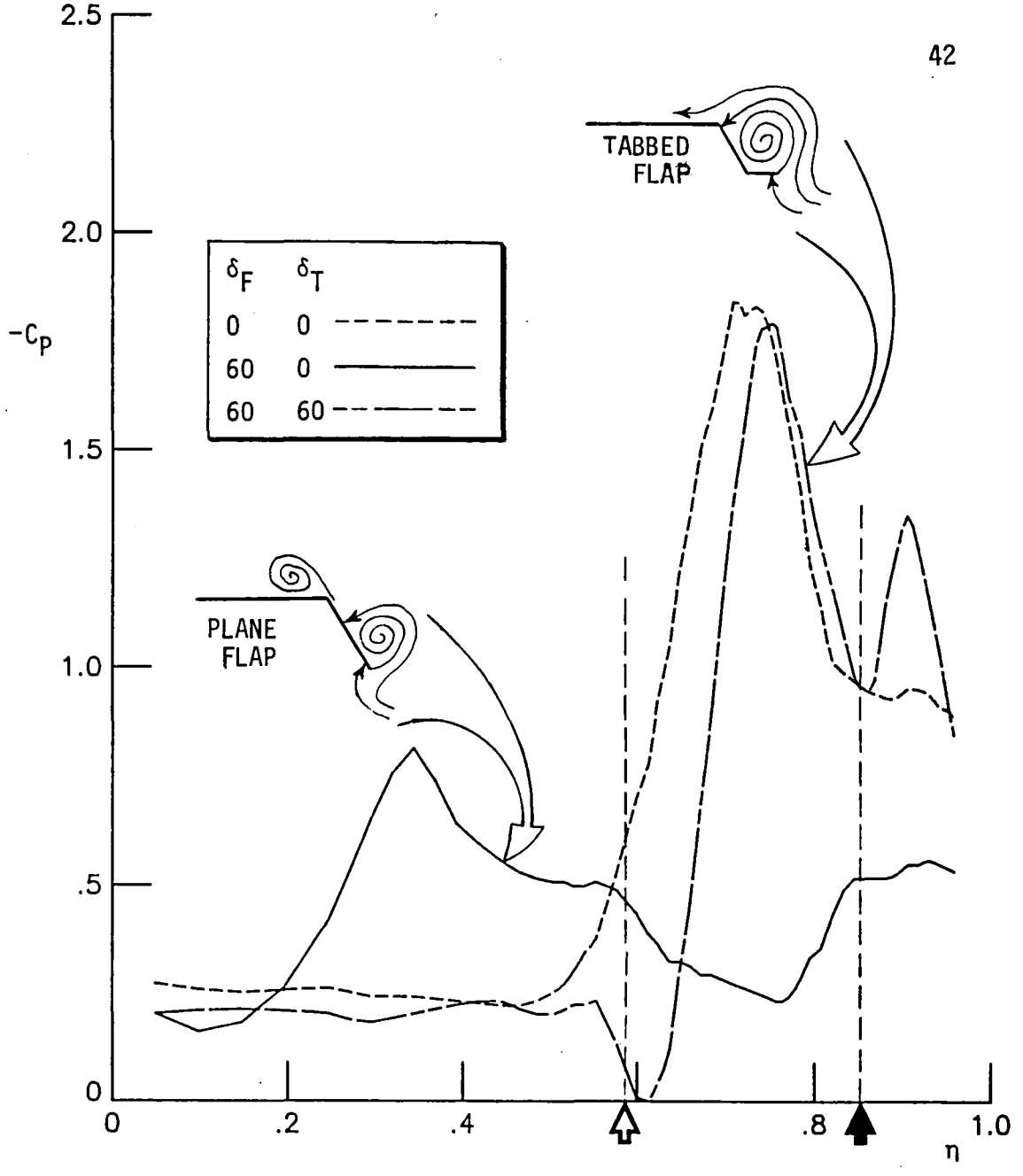

FIG. 6. (concluded)

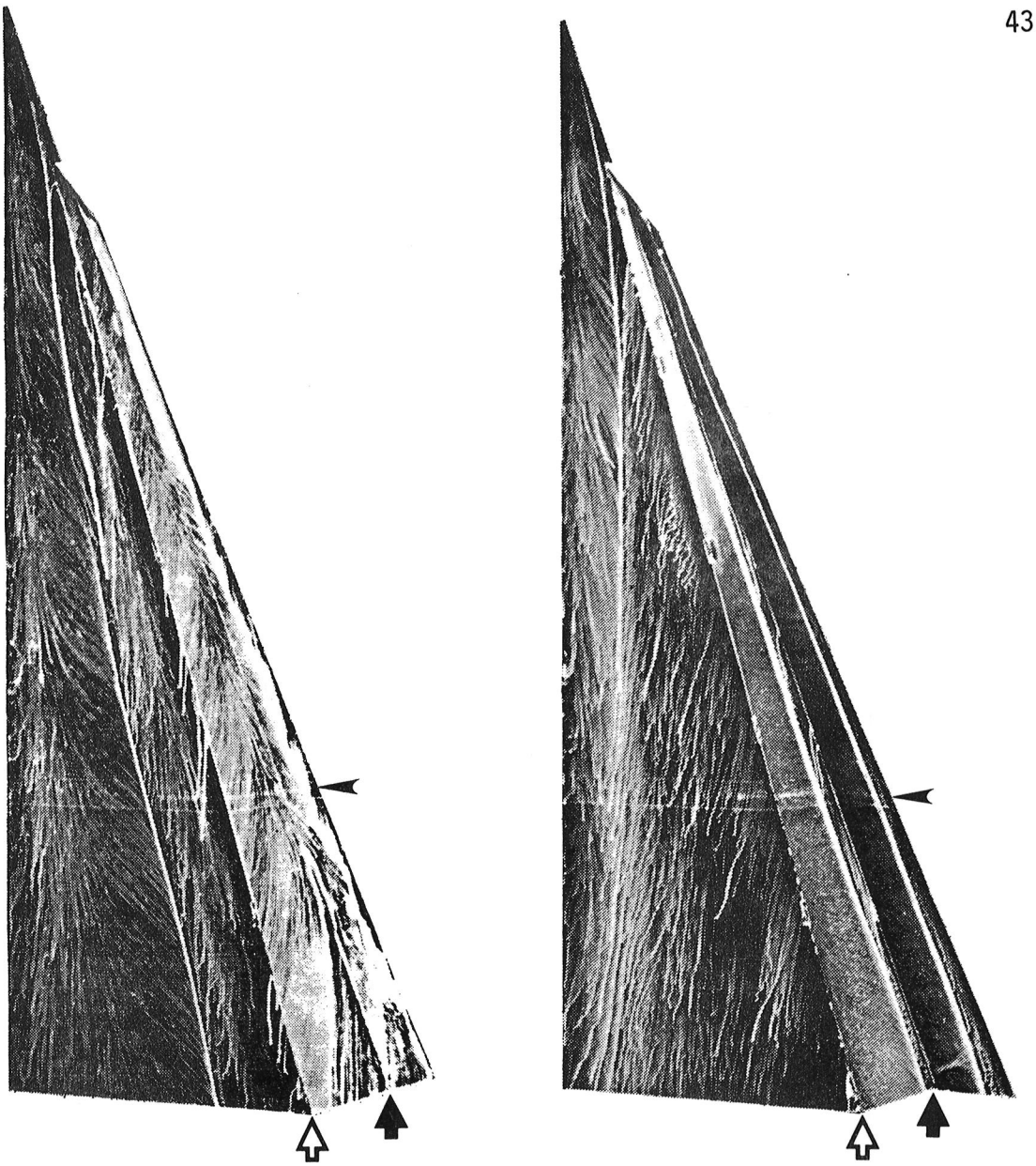

PLANE FLAP

δ_F = 60, δ_T = 0 deg.

TABBED FLAP

δ_F = 60, δ_T = 60 deg.

FIG. 7. Oil flow on 60 deg. delta with plane and tabbed flap at α = 16 deg.

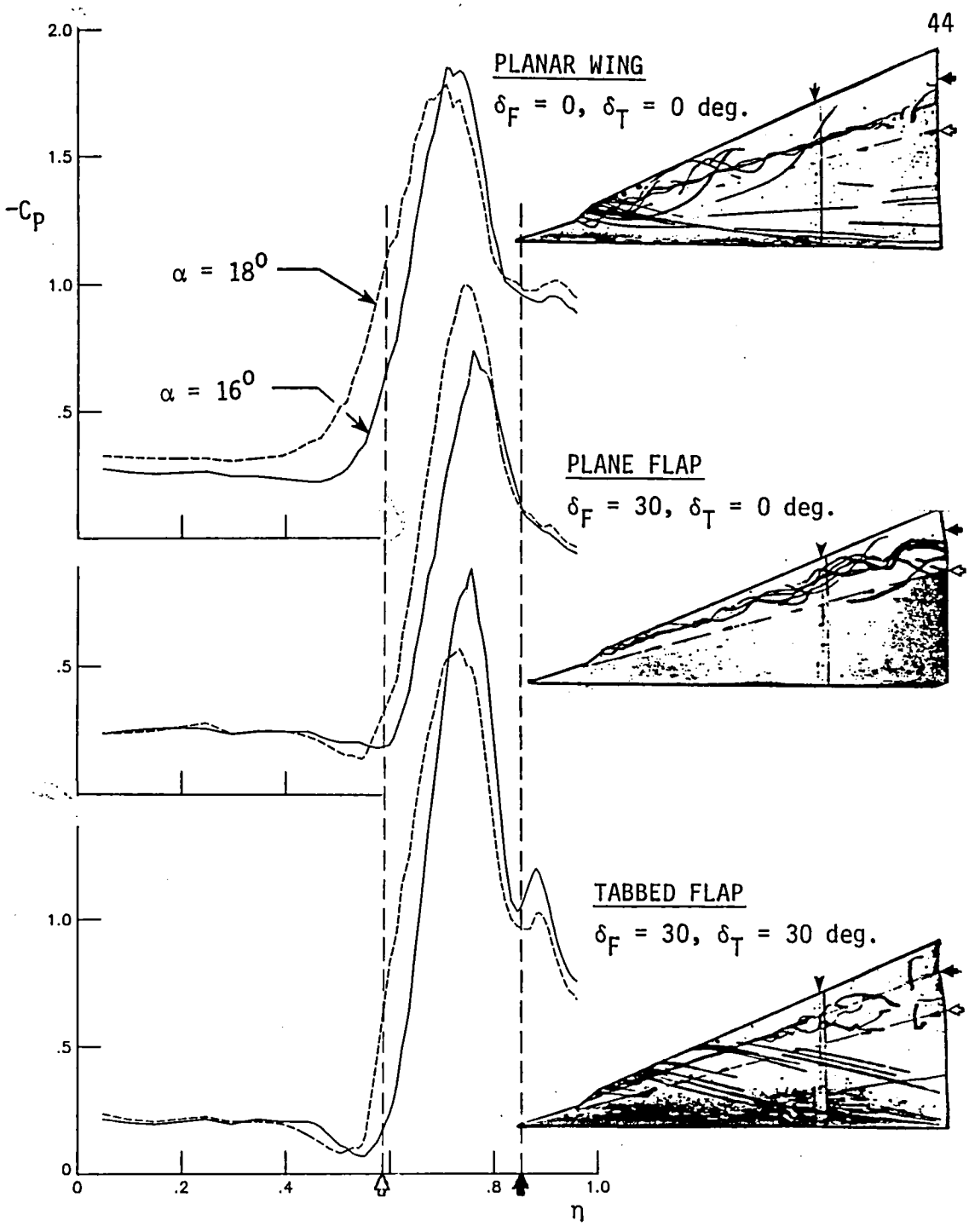

FIG. 8. Upper-surface pressure distributions at α = 16 and 18° and helium bubble photographs at α = 18°, of the planar wing, plane flap, and tabbed flap.

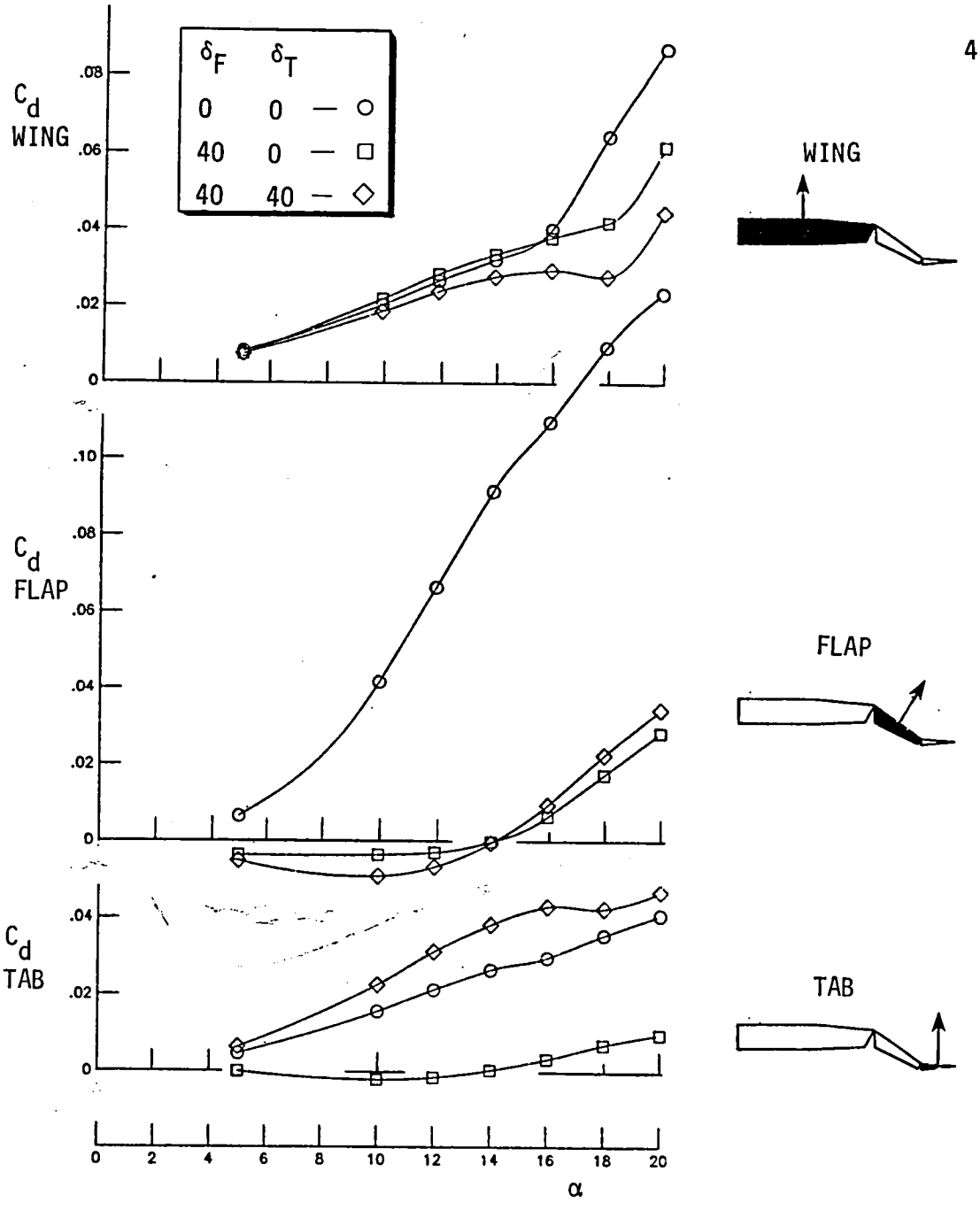

FIG. 9. Individual sectional drag contribution of wing, flap, and tab derived from upper surface pressure distributions.

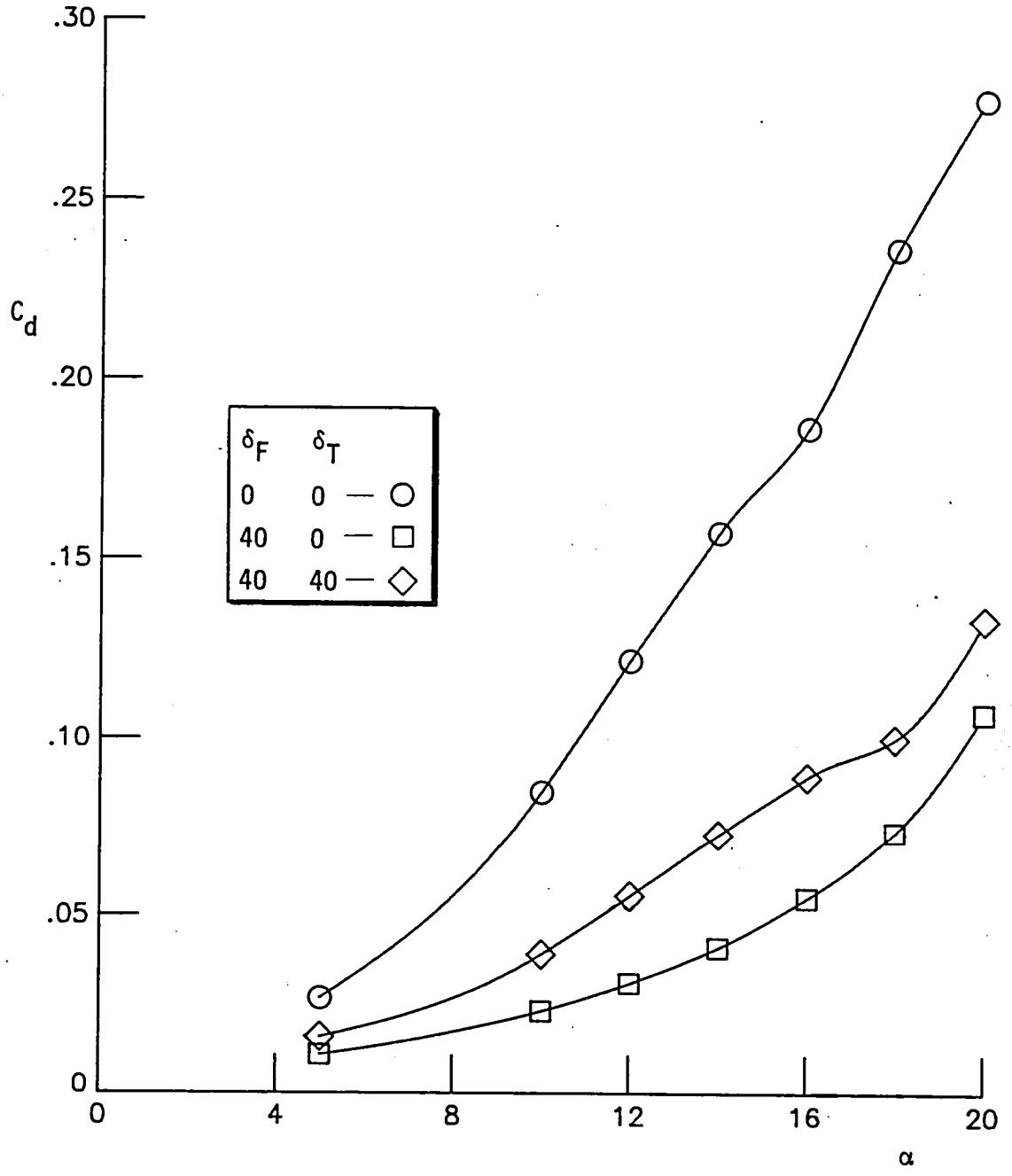

FIG. 10. Sectional configuration drag summed from the drag of wing, flap, and tab.

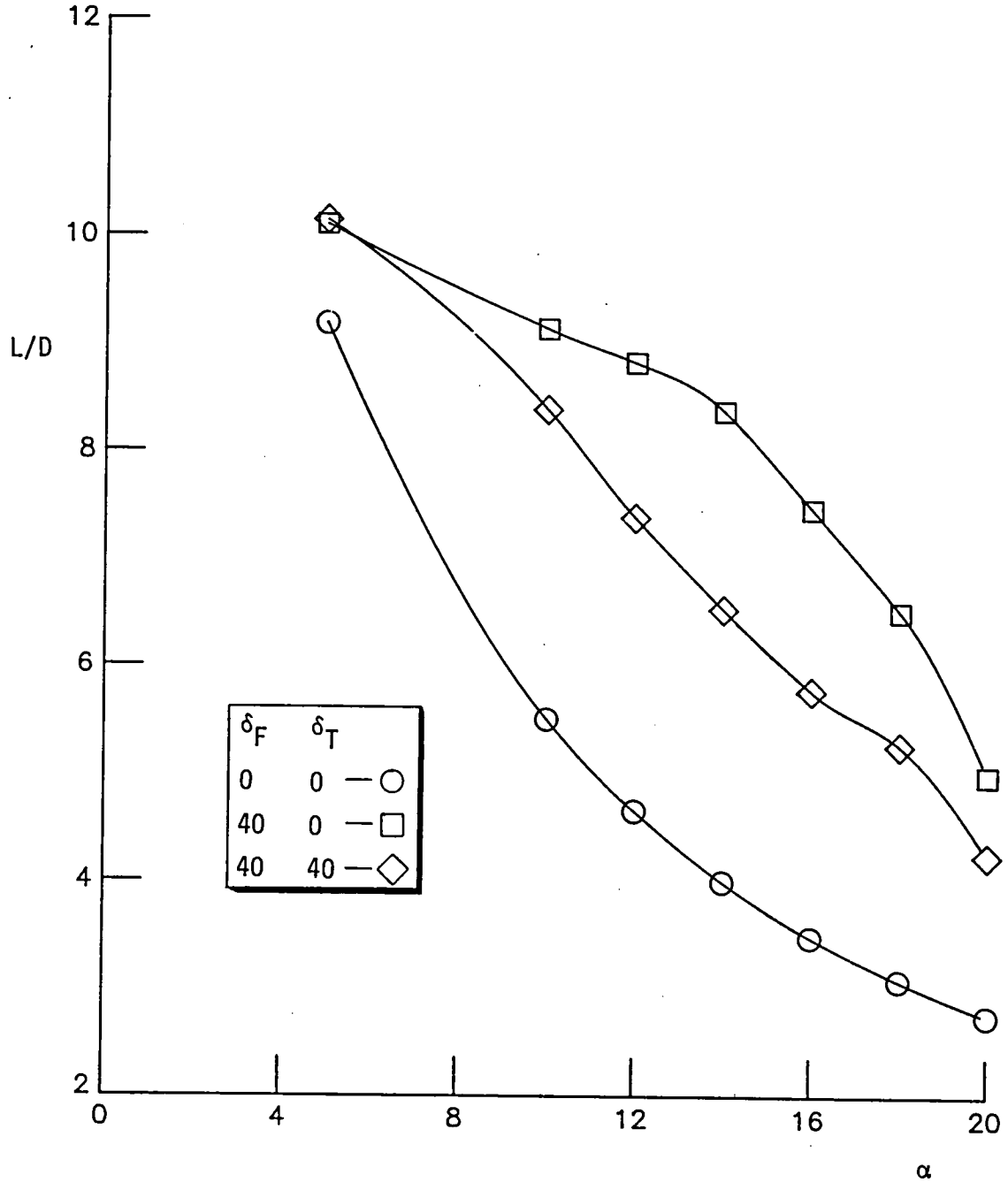

FIG. 11. Sectional L/D vs. α of 65^{o} delta model.

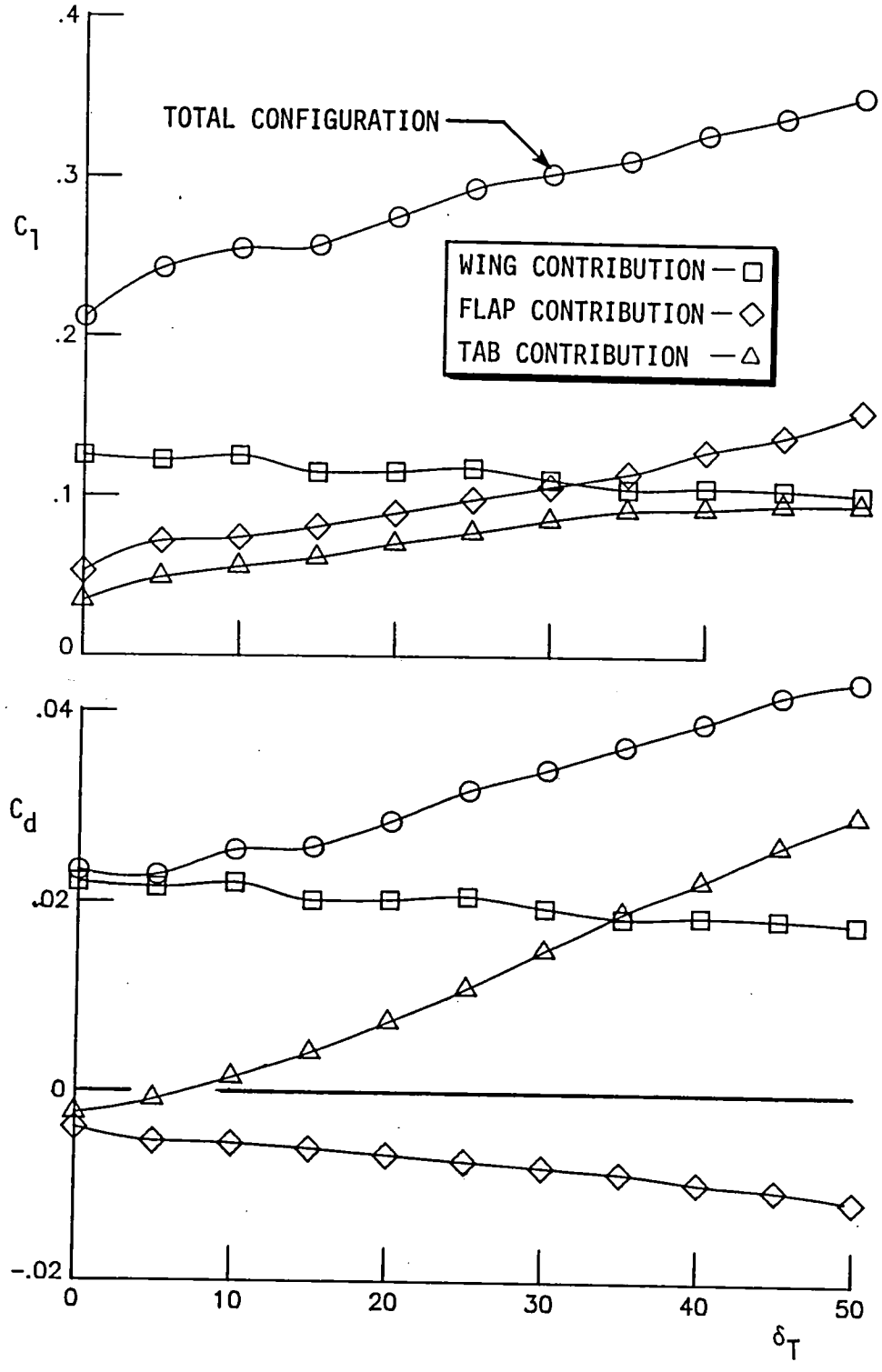

FIG. 12. Sectional lift and drag of the configuration and the individual wing, flap, and tab contributions as a function of δ_T at $\alpha = 10^o$ and $\delta_F = 40^o$.

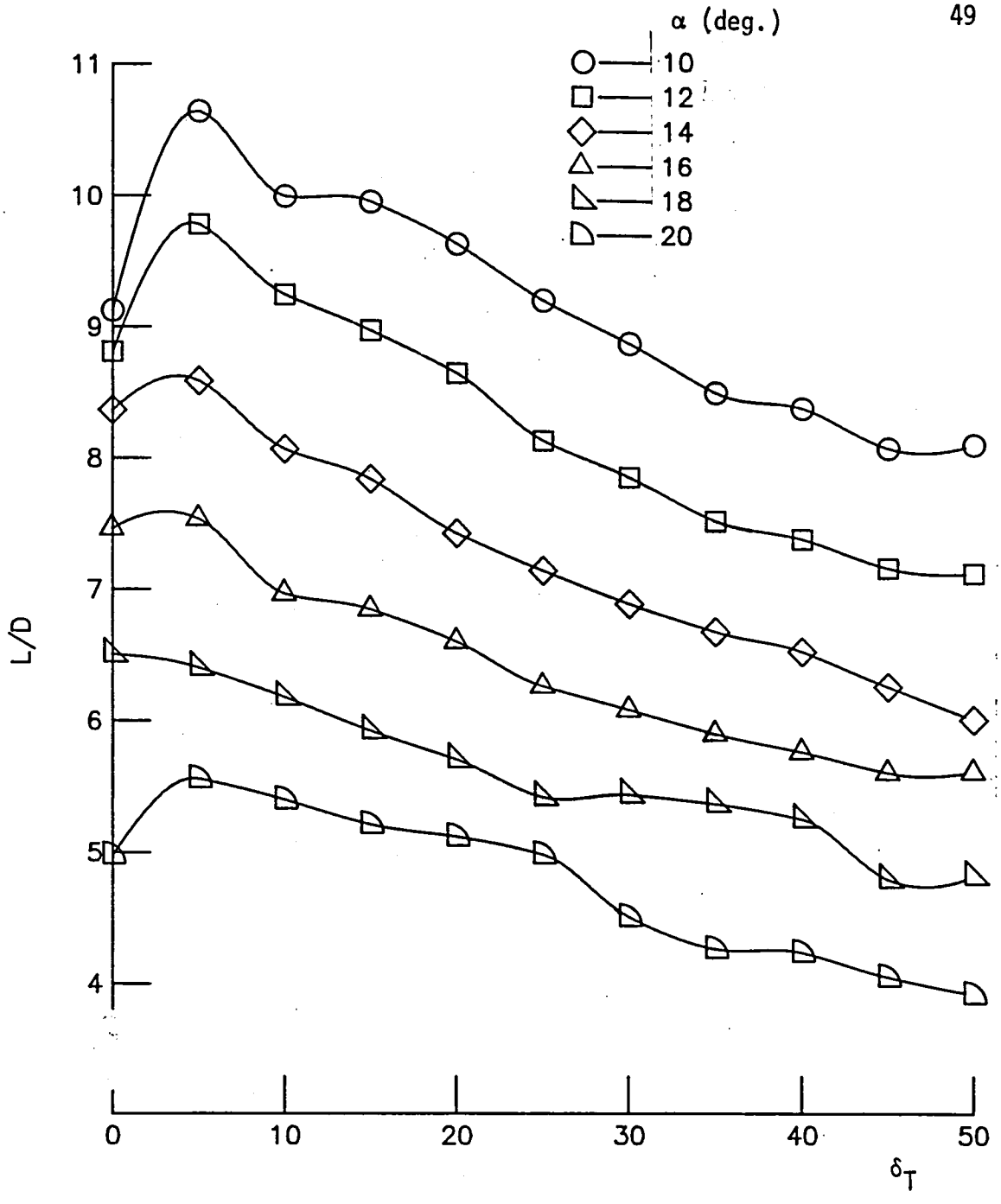

FIG. 13. Sectional L/D vs. δ_T for different α's with a constant flap deflection of 40^o.

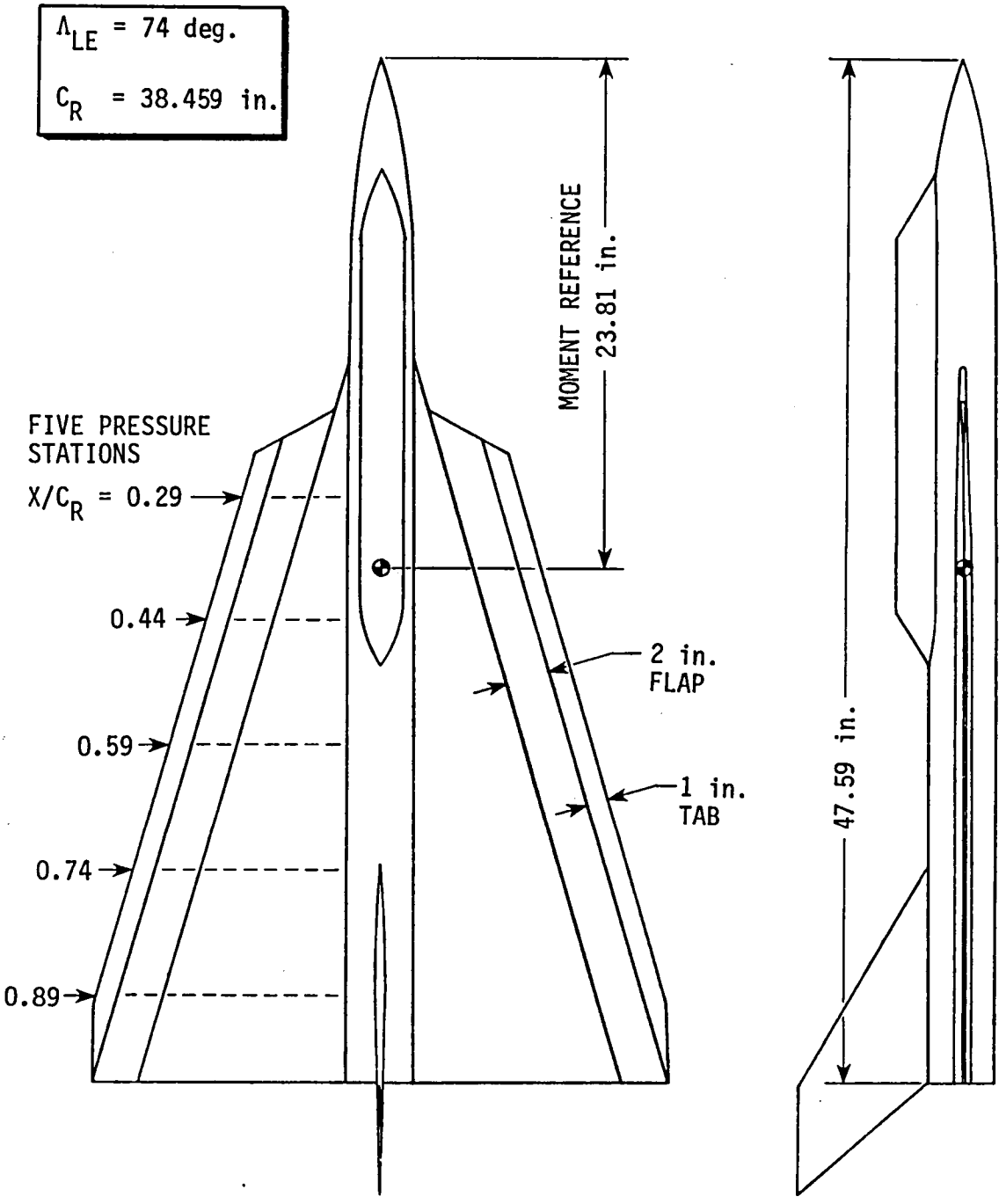

FIG. 14. 74 deg. delta wing body configuration with constant-chord flaps and baseline constant chord tabs.

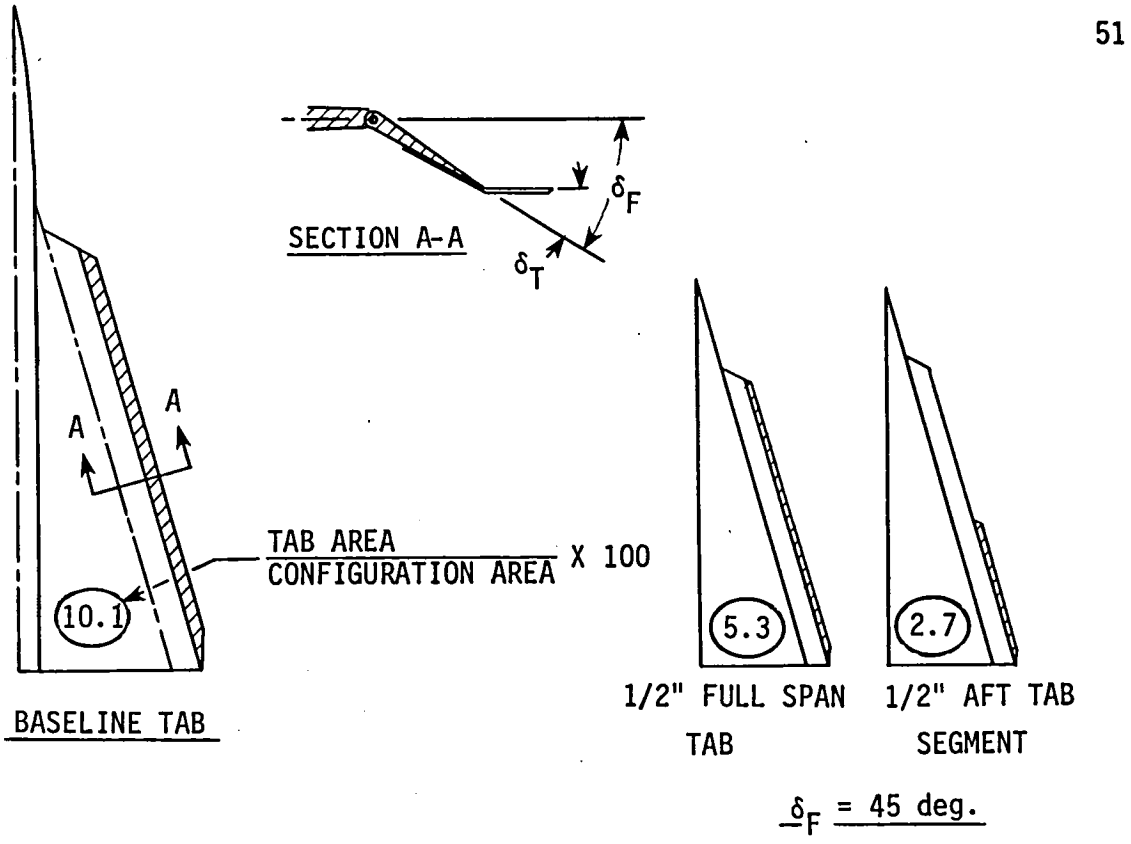

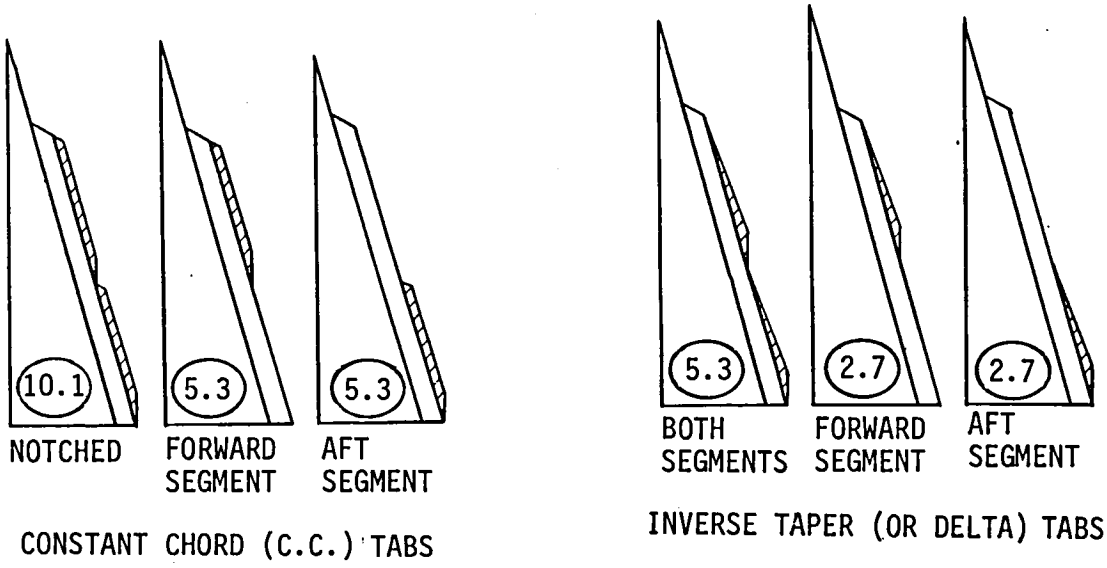

FIG. 15. Tab planform modifications tested on the 74 deg. delta model.

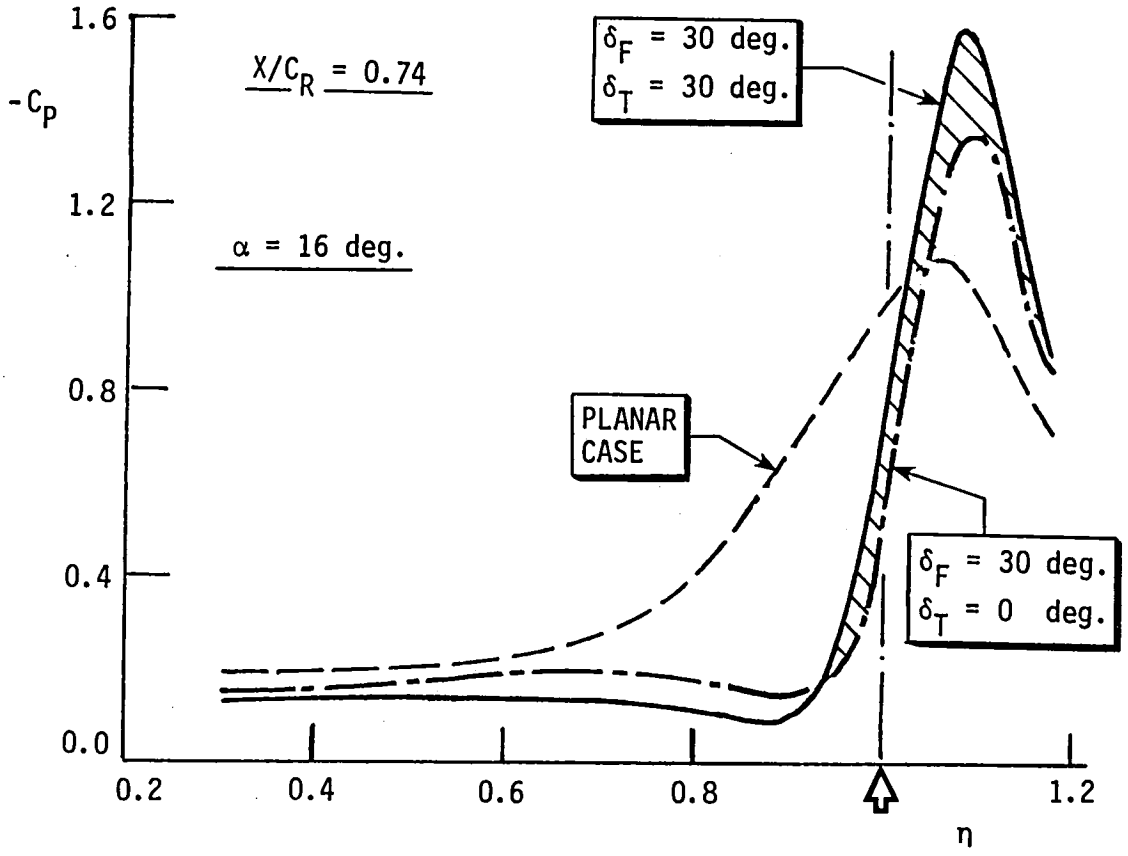

FIG. 16. C_p distribution across wing and flap on the 74 deg. delta wing (tab was uninstrumented).

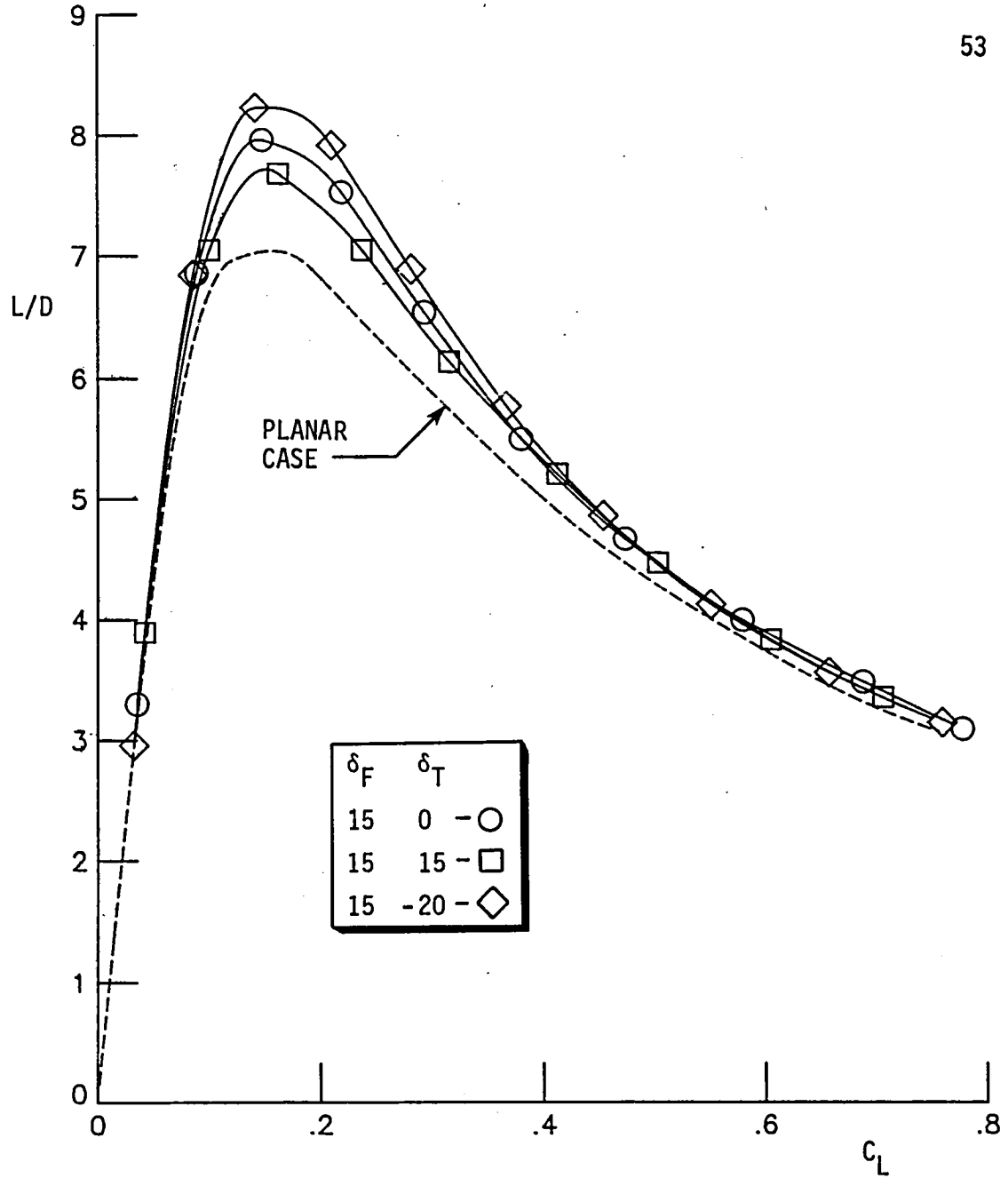

FIG. 17. L/D vs. C_L on 15 deg. plane flap and 15 deg. flap with positive and negative tab deflections.

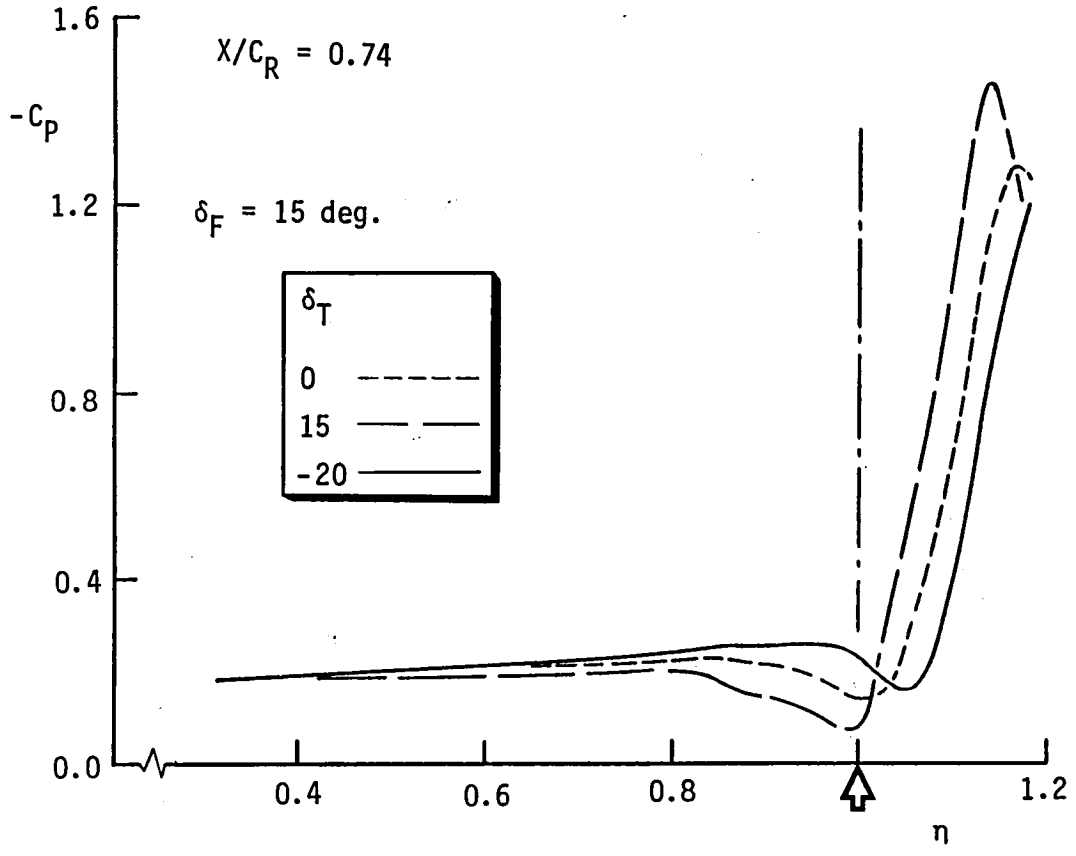

FIG. 18. C_p distribution on 15 deg. flap case with plane flap, and positive and negative tab deflections (at α = 16 deg. or C_L = 0.5).

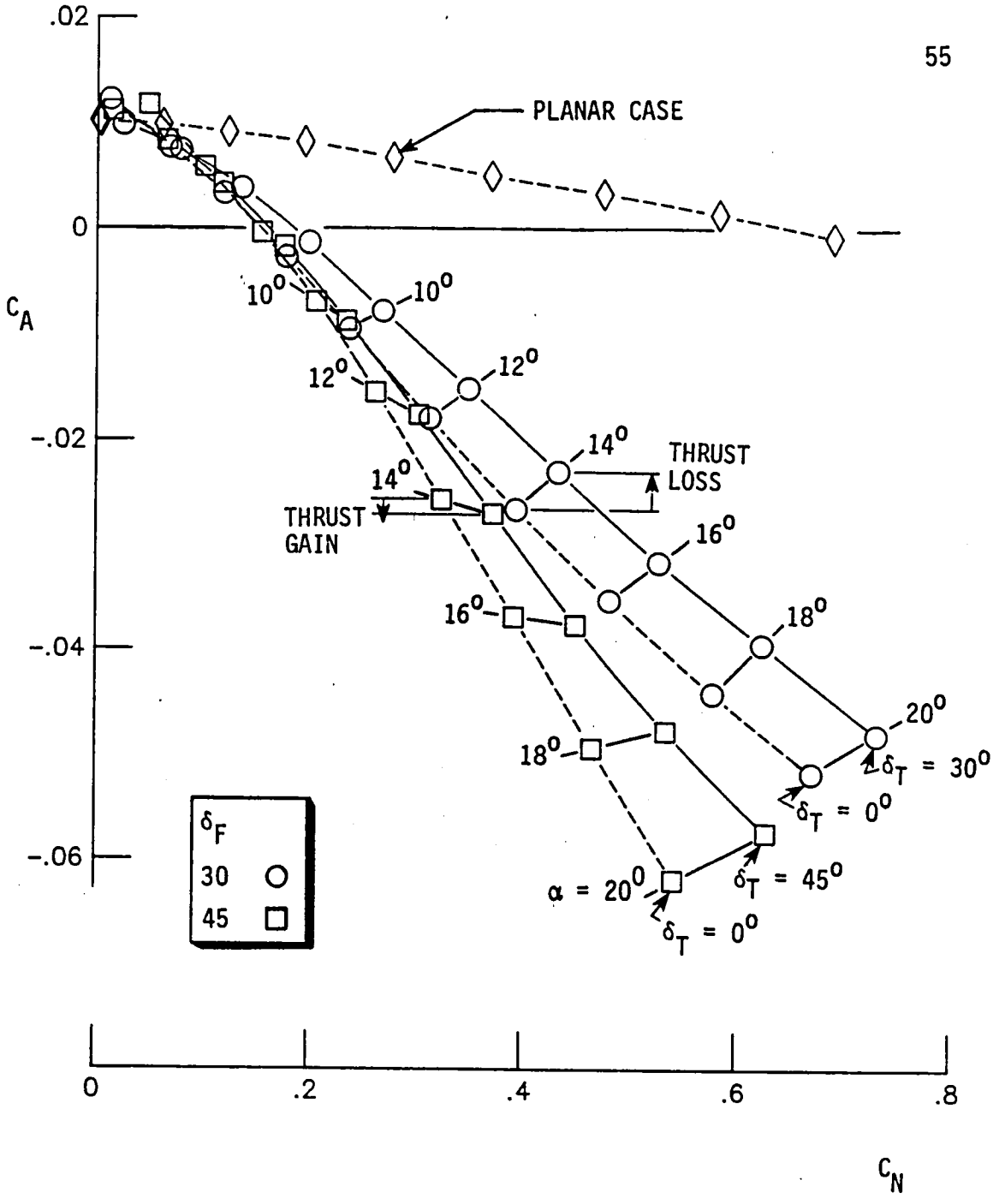

FIG. 19. Effect of tab deflection on normal and axial force coefficients.

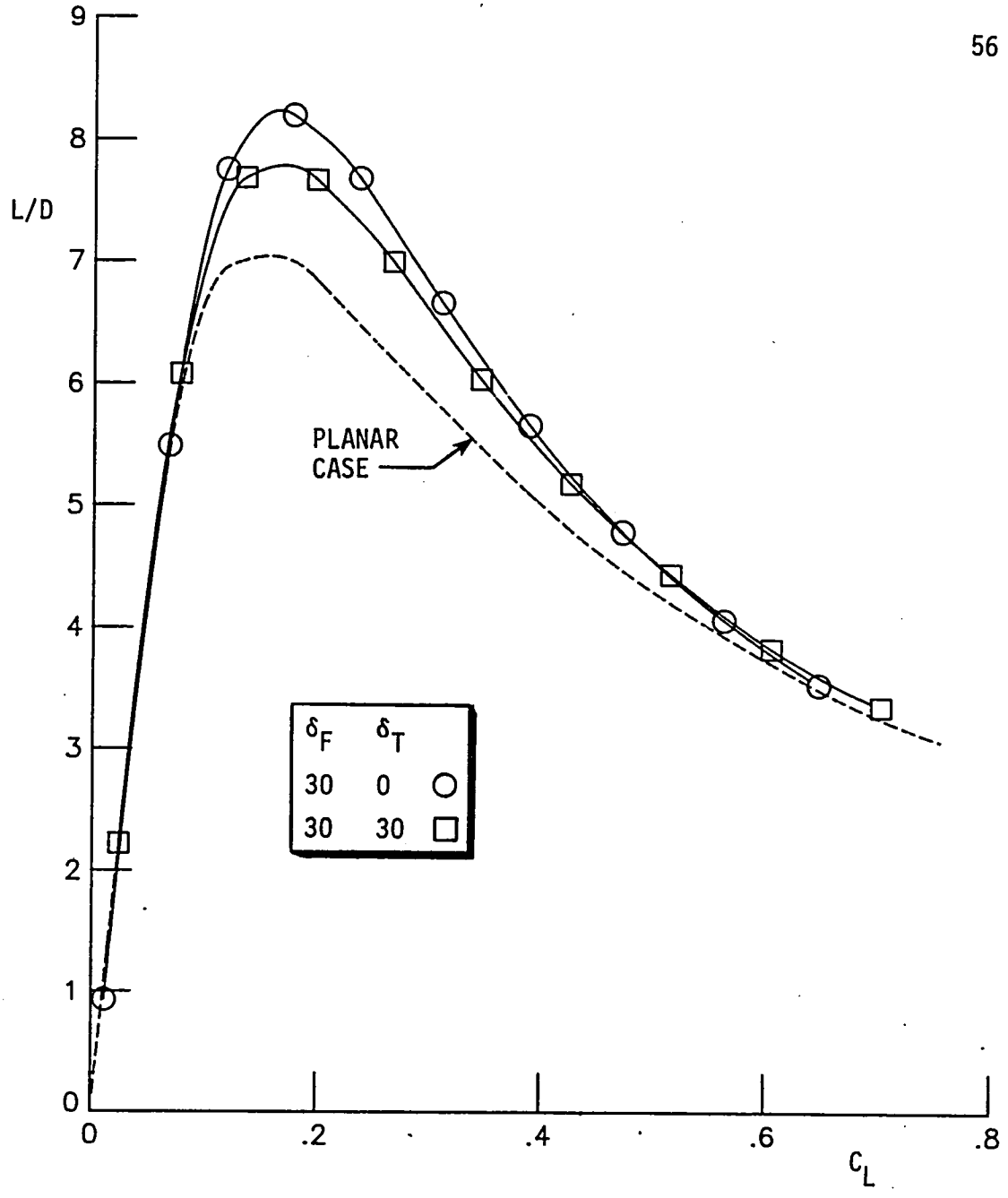

FIG. 20(a). Effect of tab deflection on L/D vs. C_L with δ_F = 30 deg.

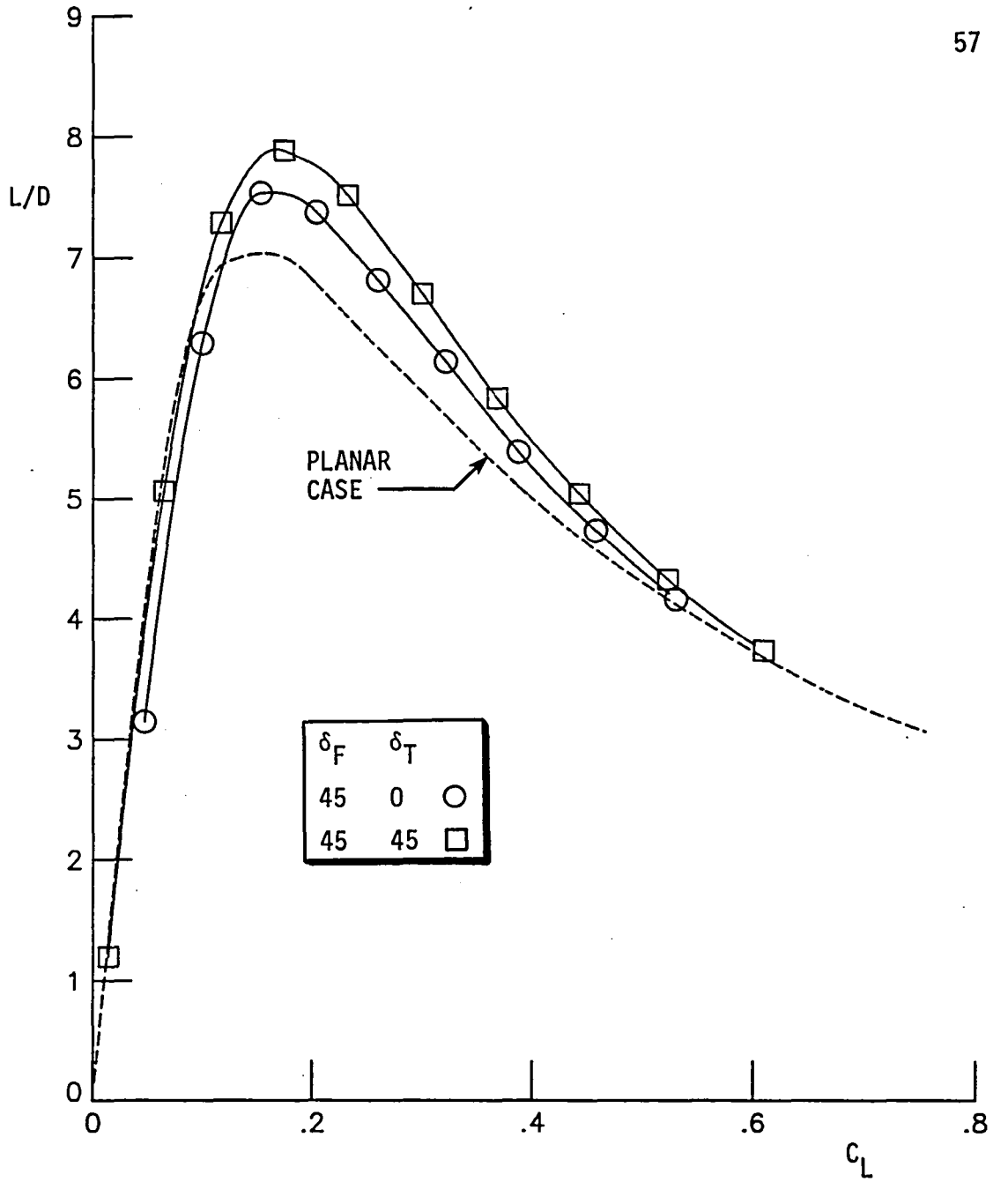

FIG. 20(b). δ_F = 45 deg.

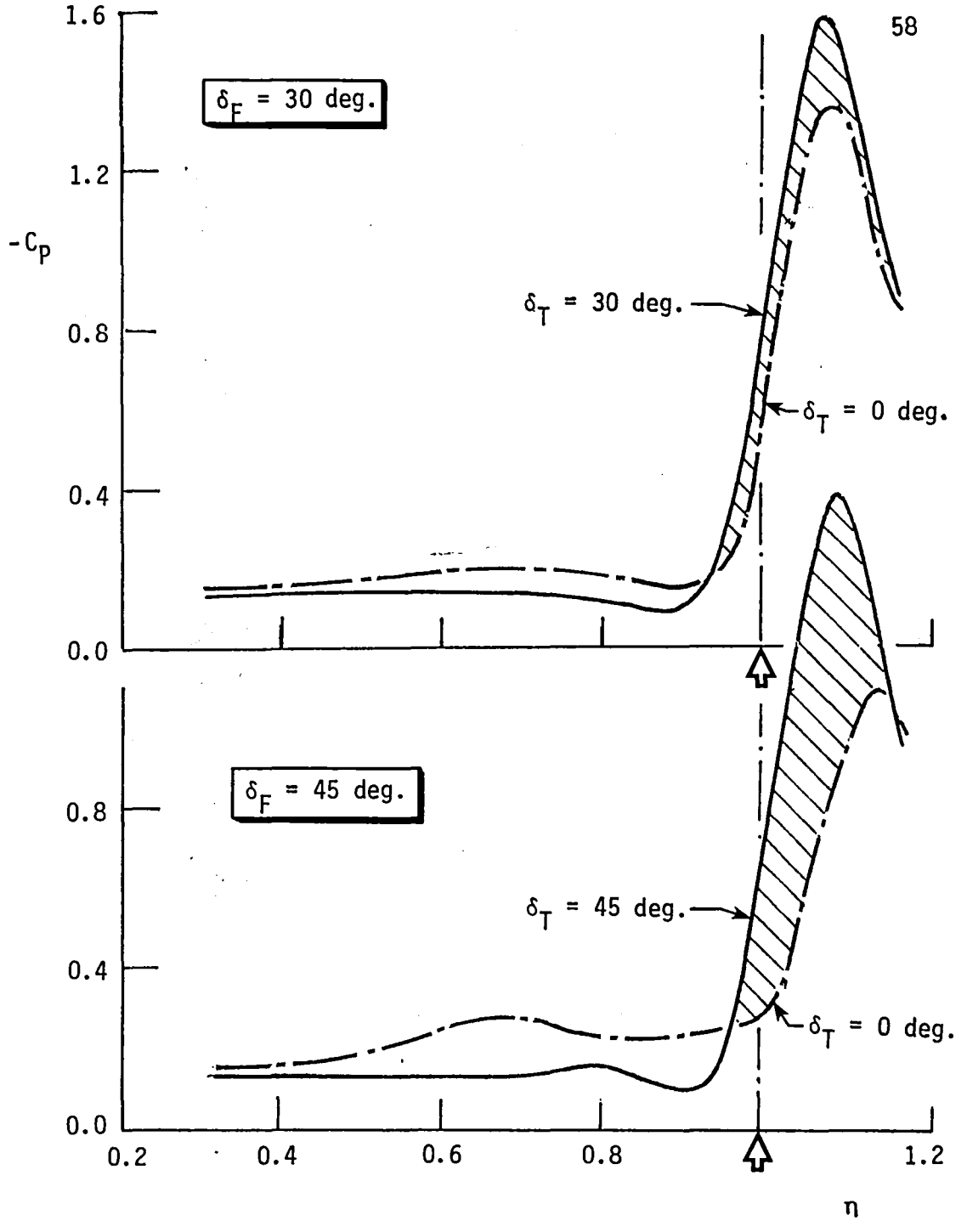

FIG. 21. Effect of δ_T and C_p distribution with δ_F = 30° and 45° at α = 16° (X/C_R = 0.74).

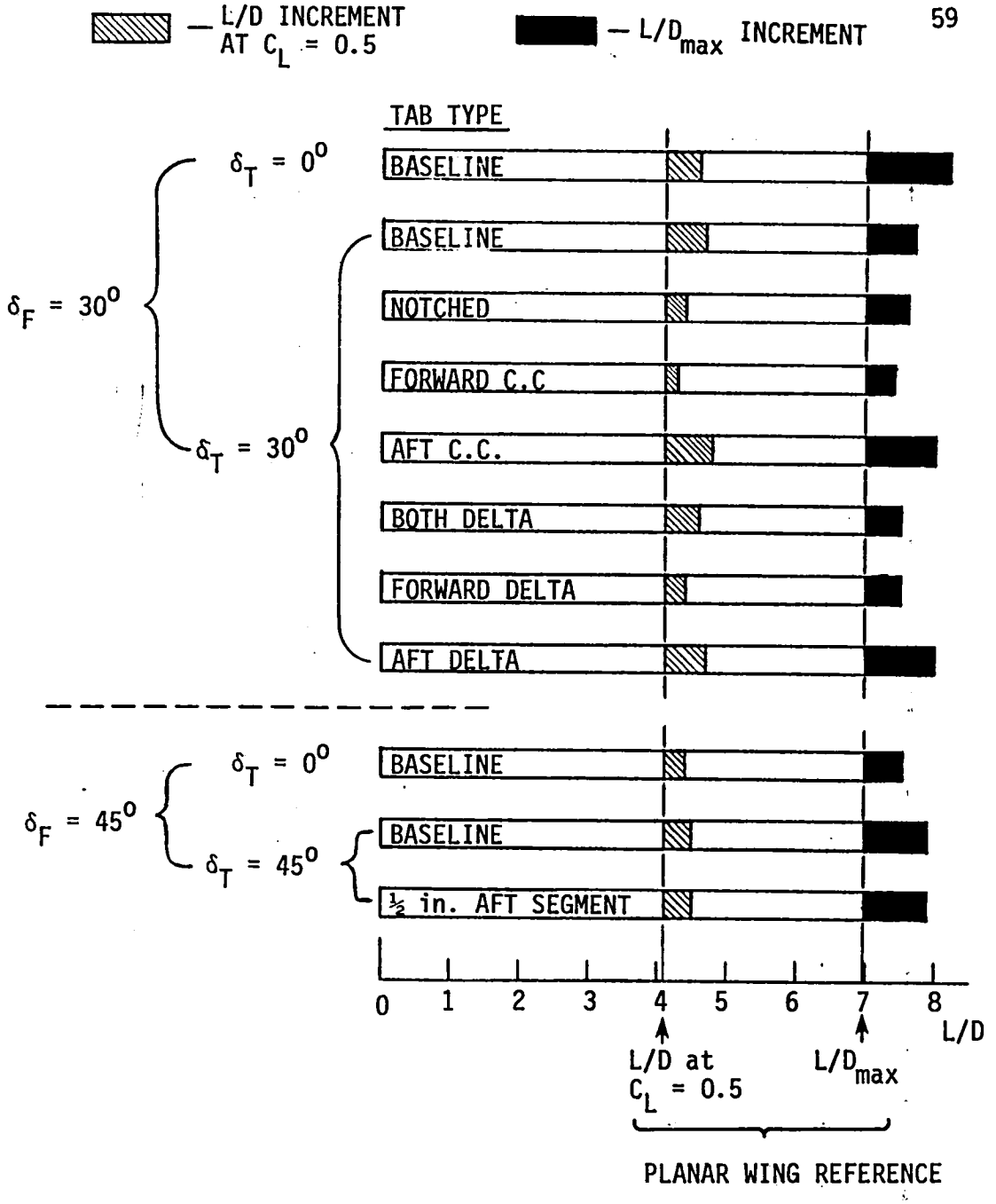

FIG. 22. Summary of tab modification effects on L/D characteristics of 74° delta model.

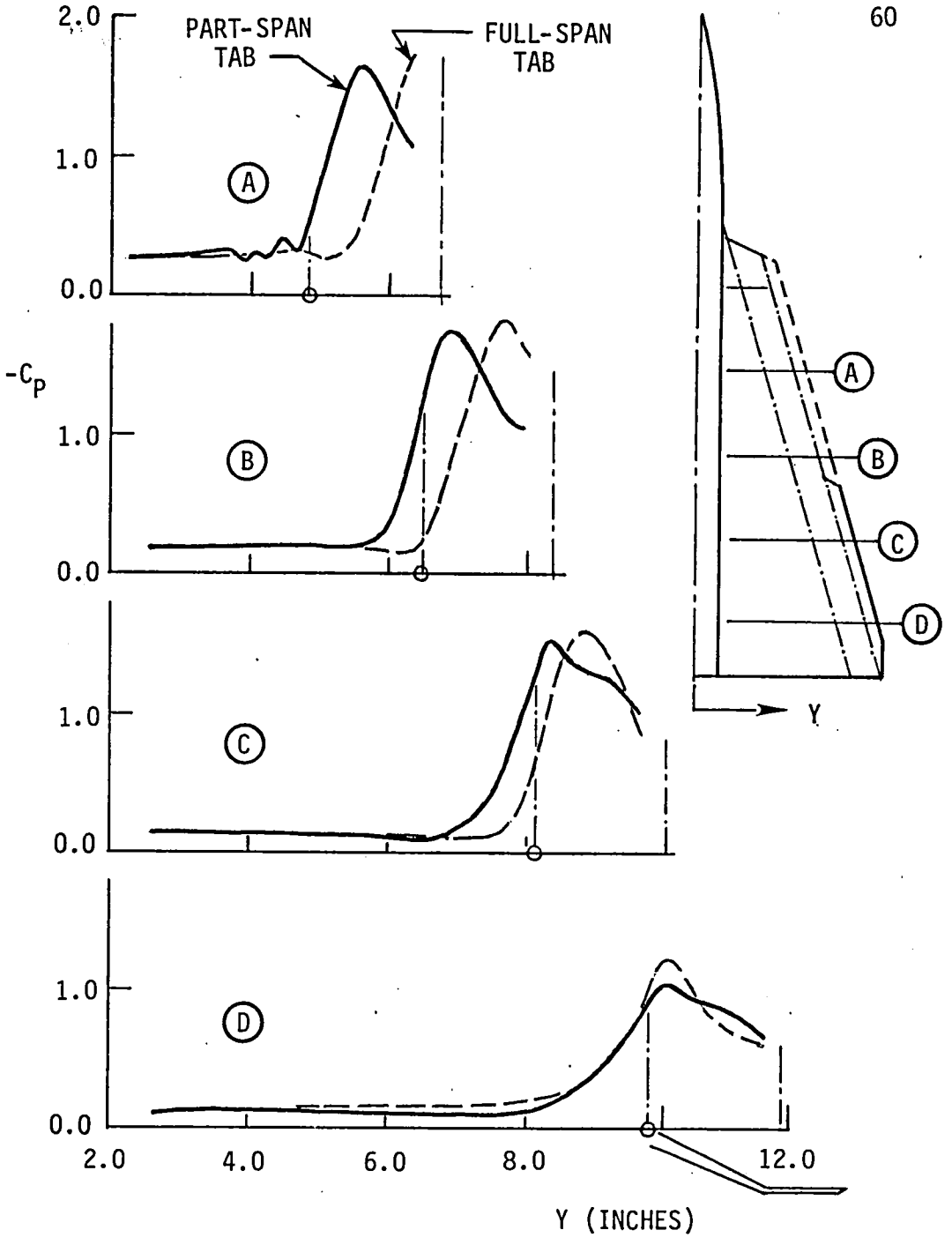

FIG. 23(a). Upper-surface pressures on 74-deg. delta -- part-span aft tab vs. baseline tab.
(δ_F = 30 deg., δ_T = 30 deg., α = 16 deg.)

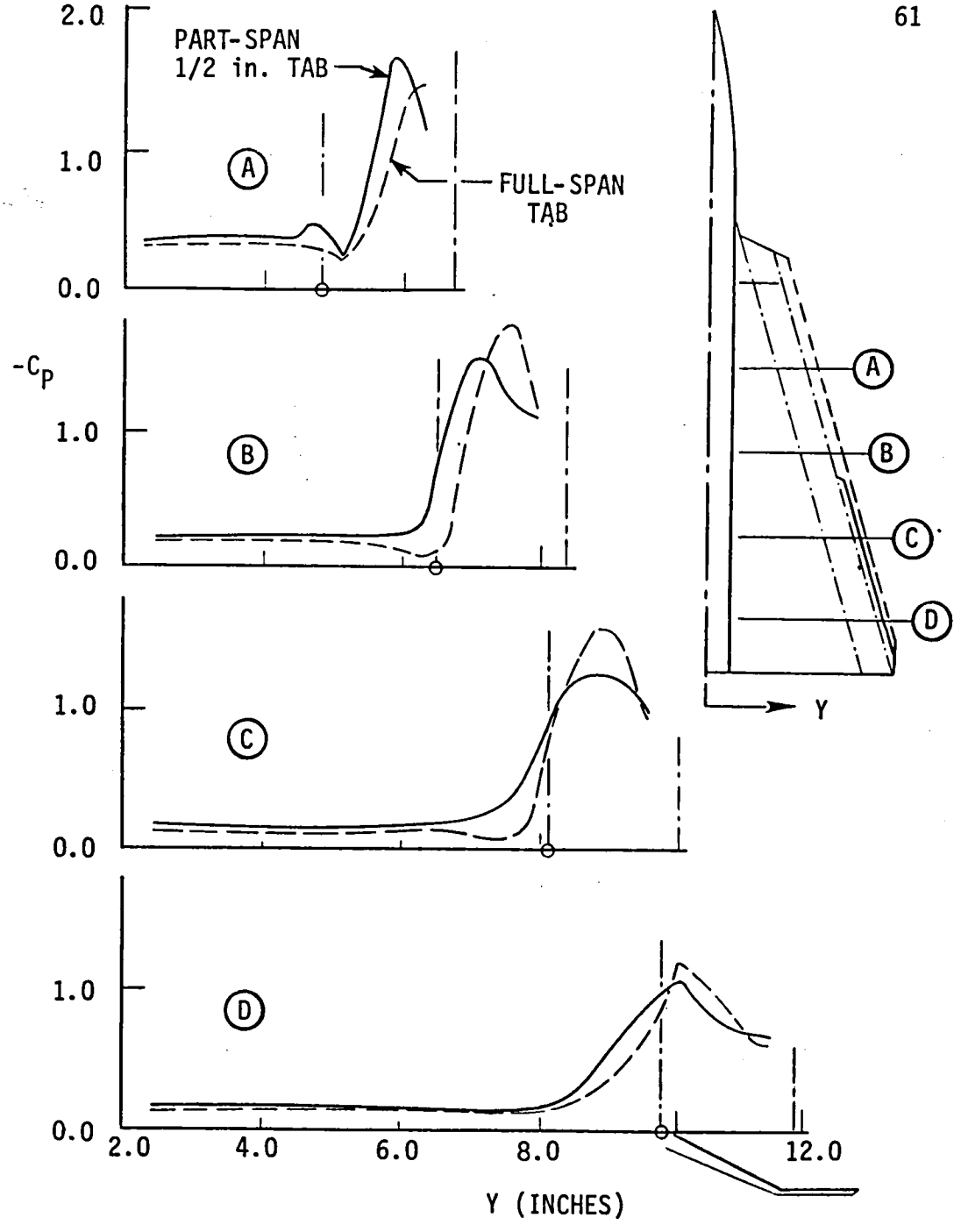

FIG. 23(b). Upper-surface pressure distribution with 1/2 in. aft tab vs. baseline tab.
(δ_F = 45 deg., δ_T = 45 deg., α = 16 deg.)

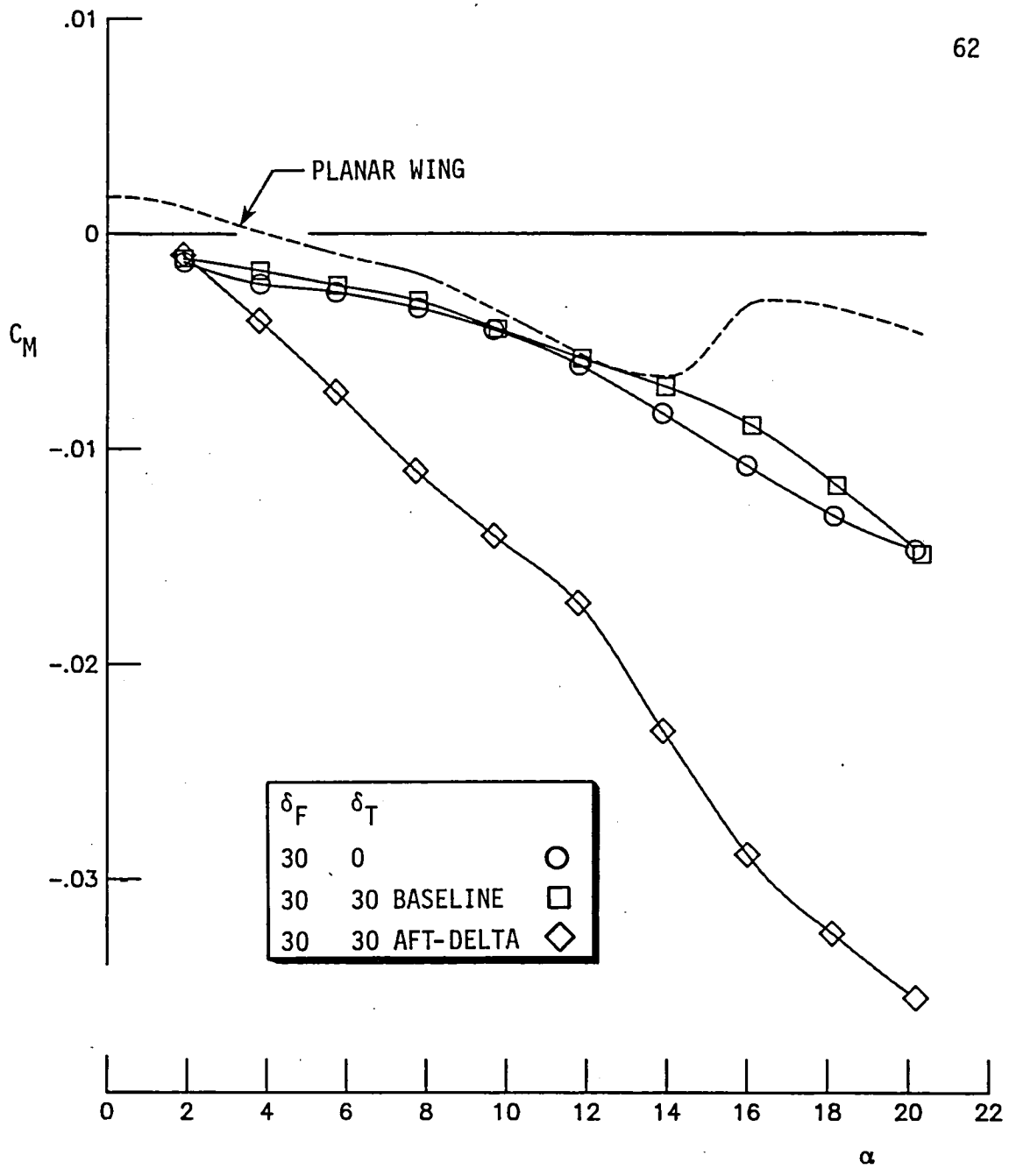

FIG. 24. Plane flap, baseline tab, and aft-delta tab effect on pitch characteristics of the 74-deg. delta.

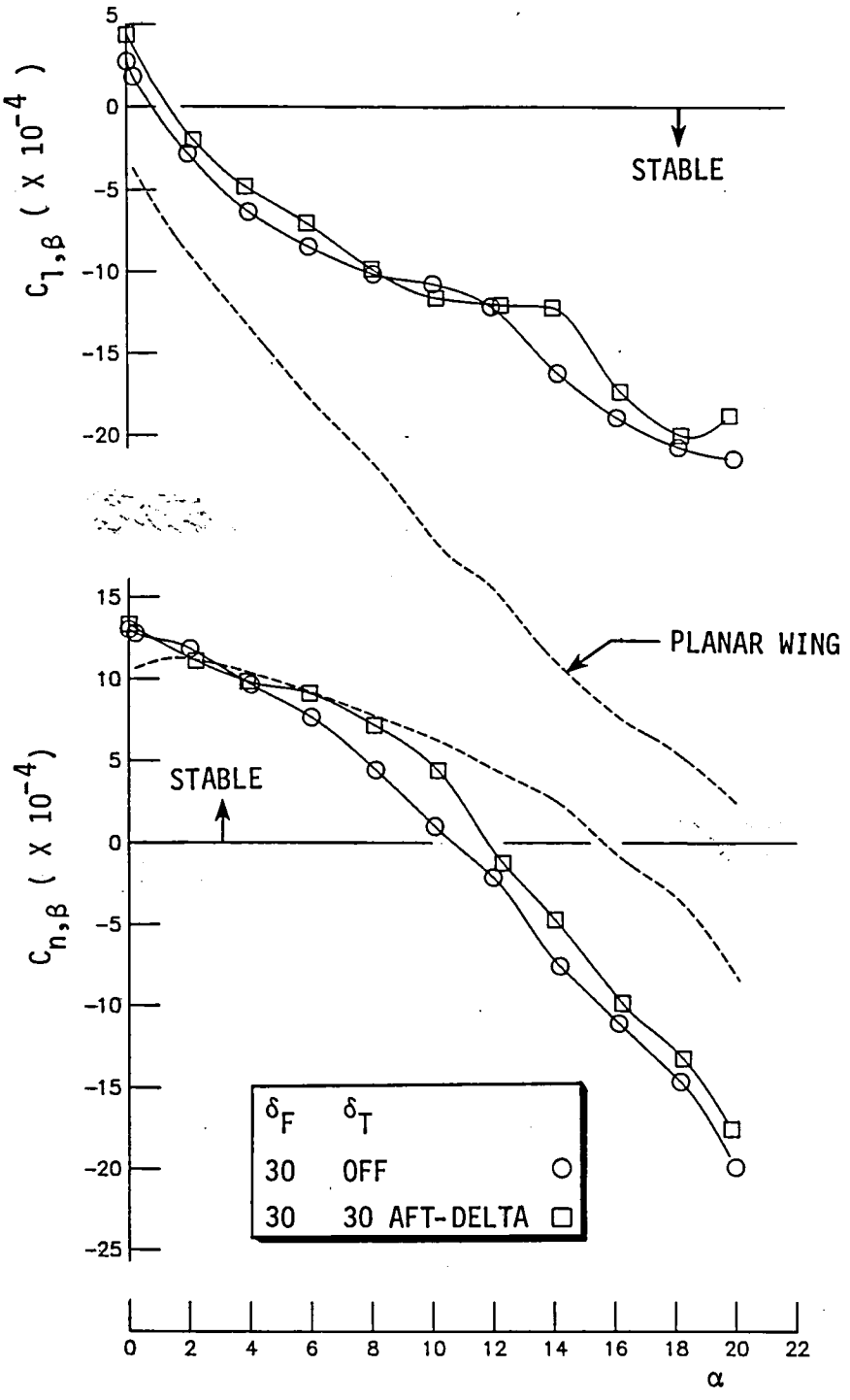

FIG. 25. Lateral directional characteristics of plane flap and aft-delta tabbed flap on 74-deg. delta.

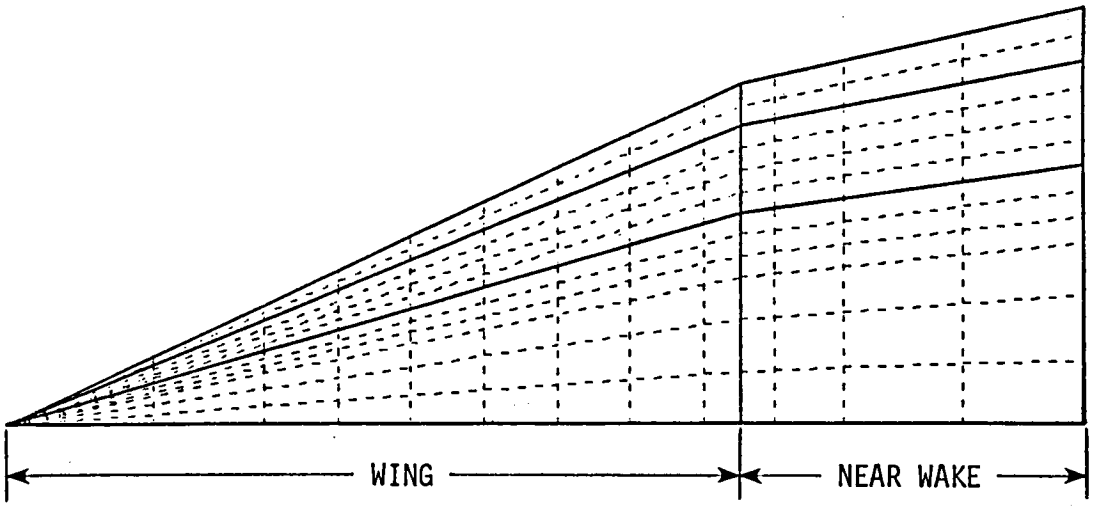

(a) Paneling of wing, flap, tab, and associated near wakes.

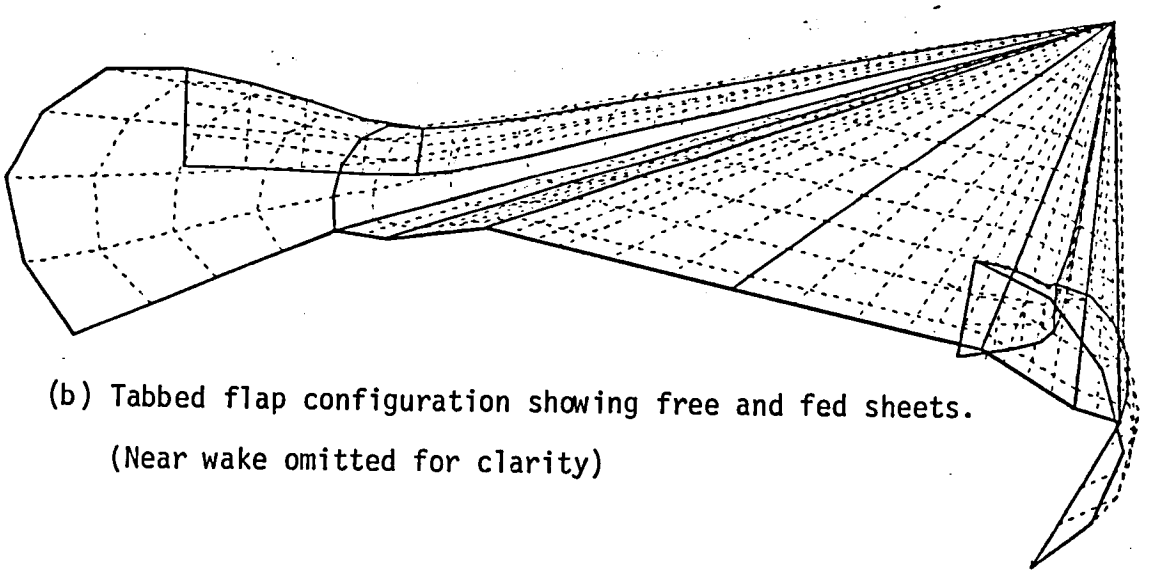

(b) Tabbed flap configuration showing free and fed sheets.
(Near wake omitted for clarity)

FIG. 26. Free vortex sheet numerical model of NCSU 65-deg. delta.

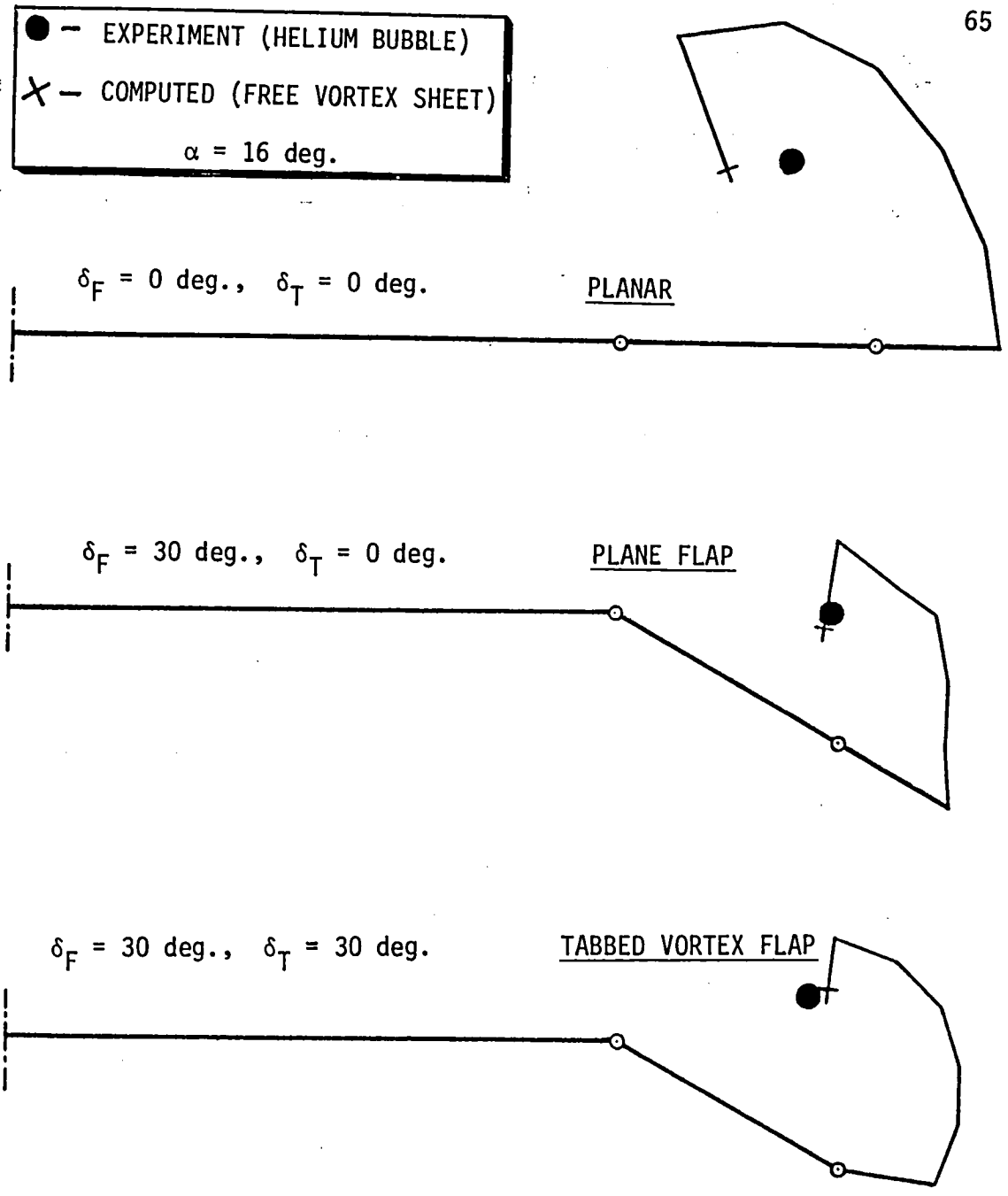

FIG. 27. Comaprison of theoritical and experimental vortex core locations on 65-deg. delta.

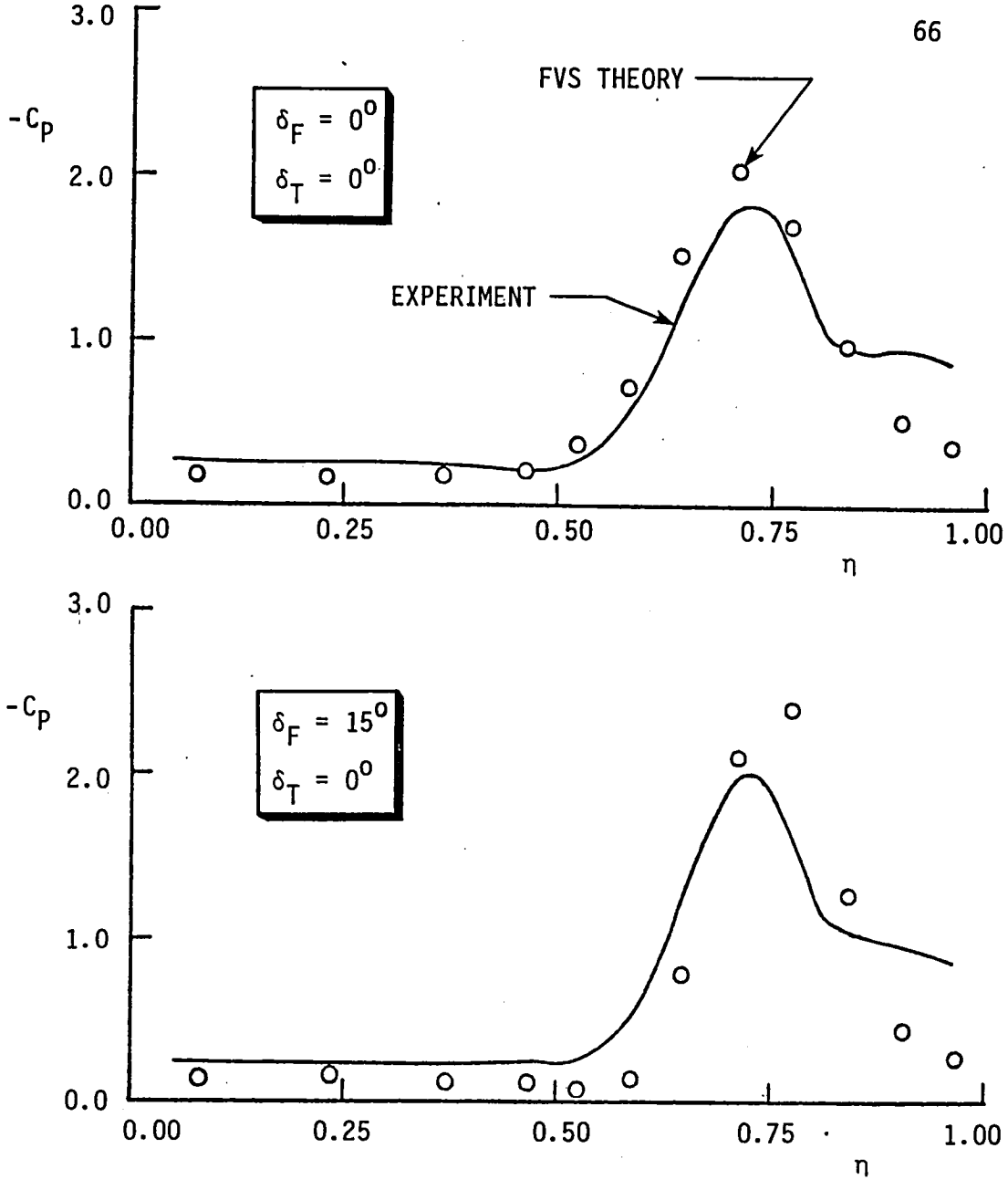

FIG. 28. Comparison of experimental and theoretical upper-surface pressure distributions at α = 16 deg.

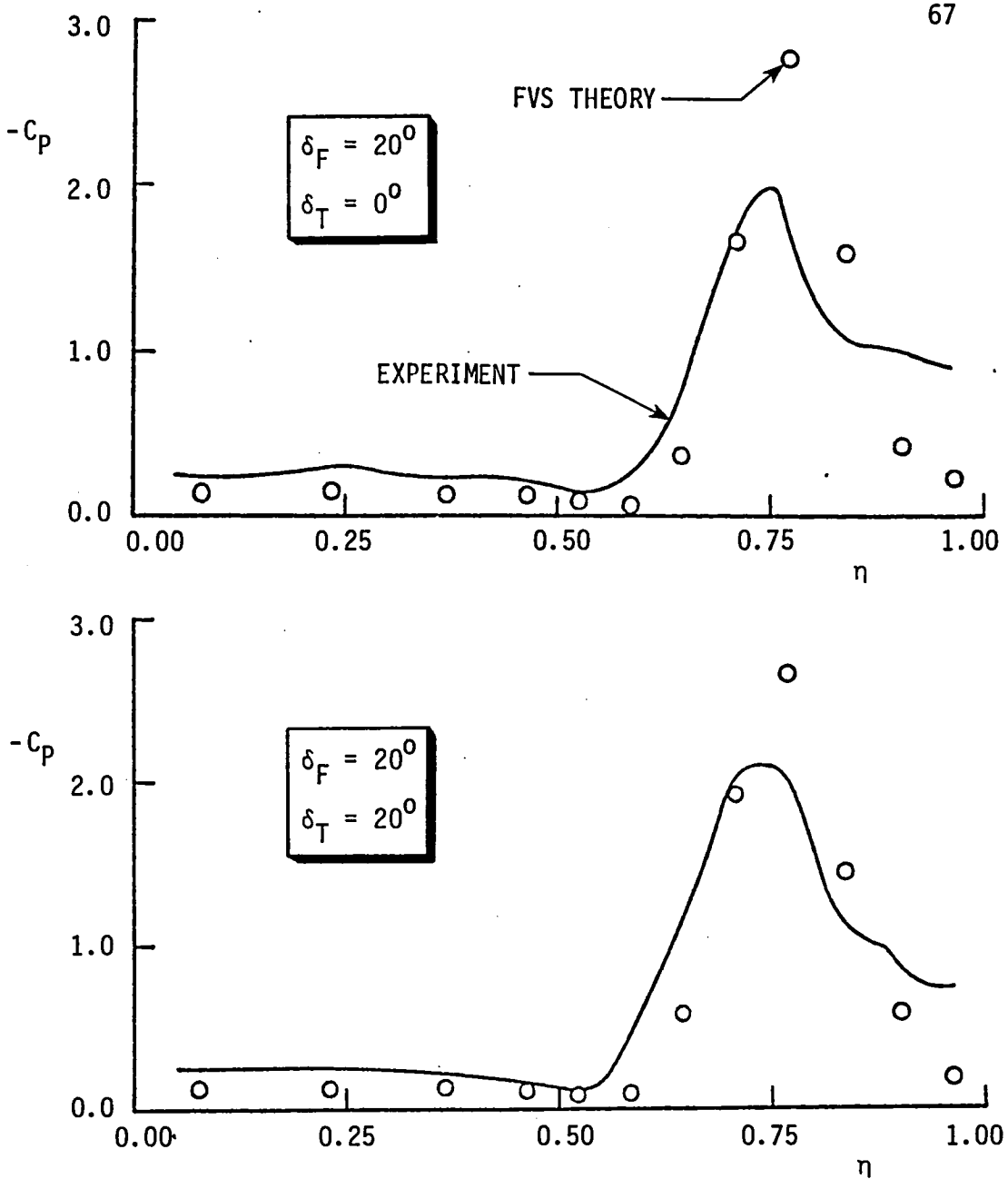

FIG. 28. (Continued)

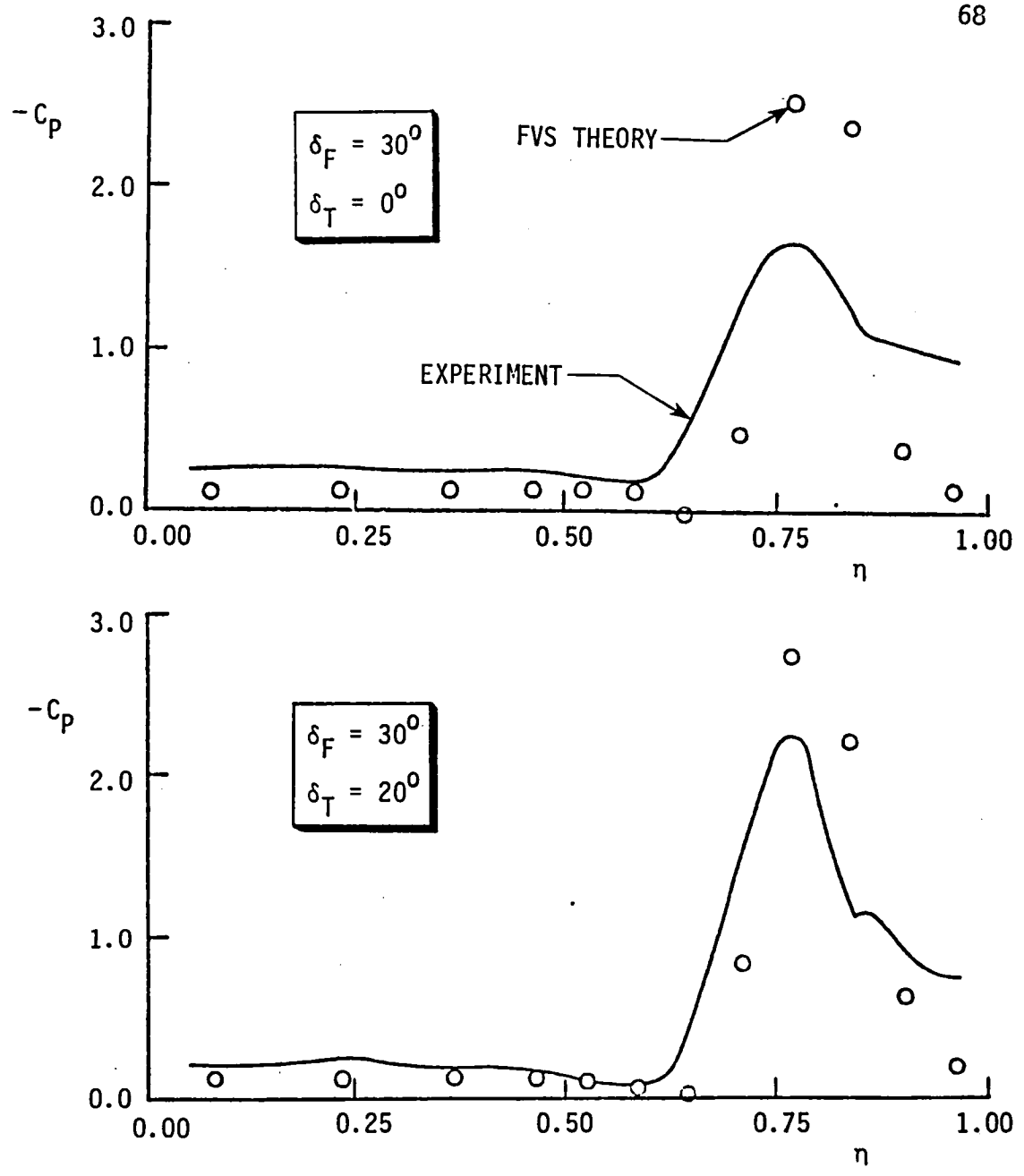

FIG. 28. (Continued)

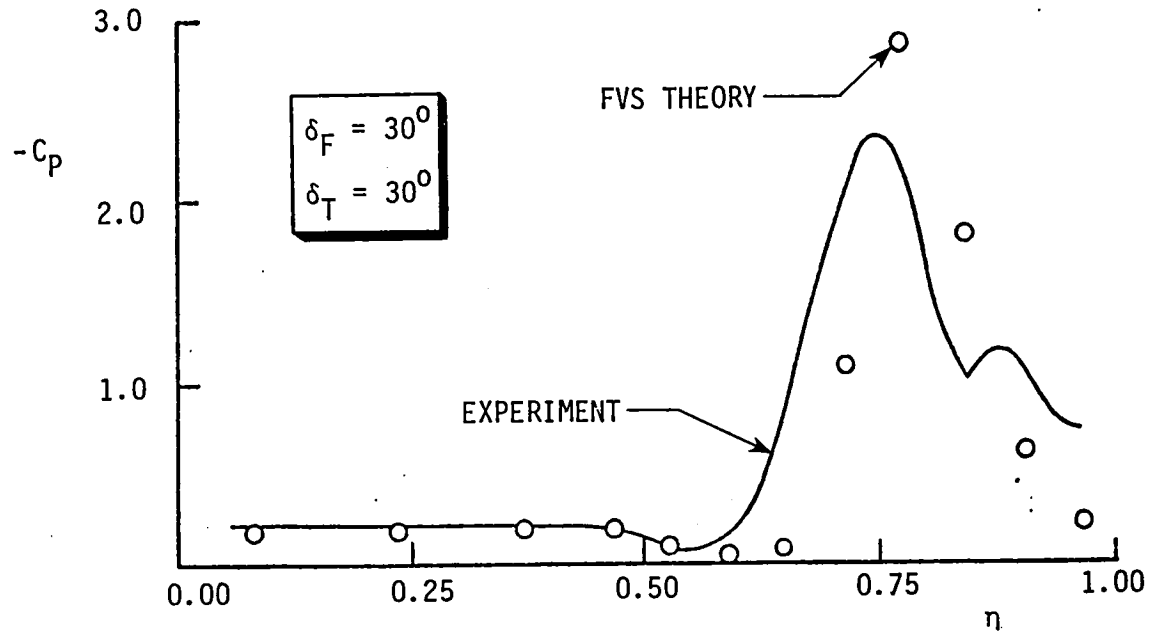

FIG. 28. (concluded)

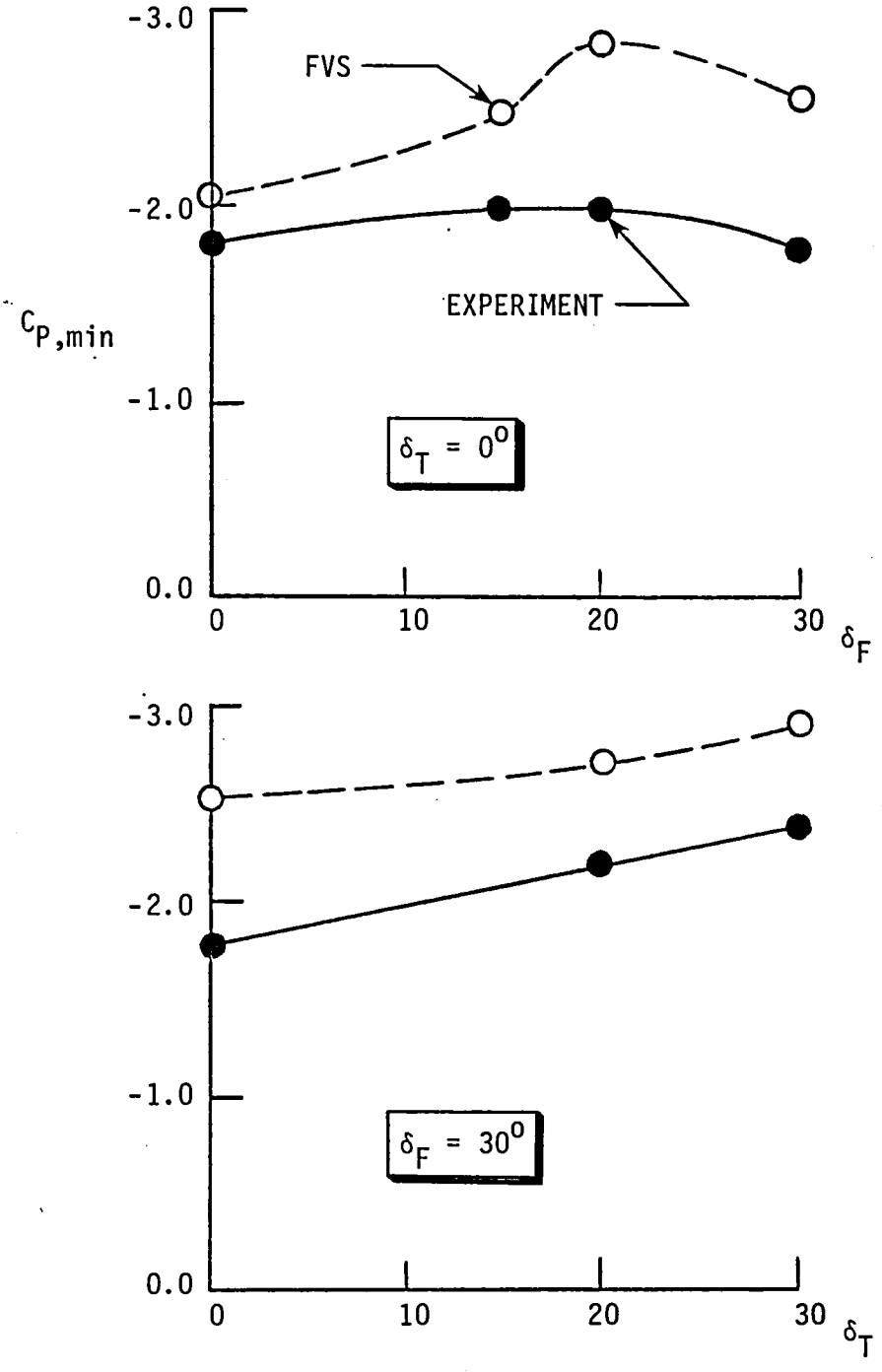

FIG. 29. Suction peak ($C_{P,min}$) as influenced by plain flap and flap + tab deflections -- Theory vs. Experiment ($\alpha = 16^o$).

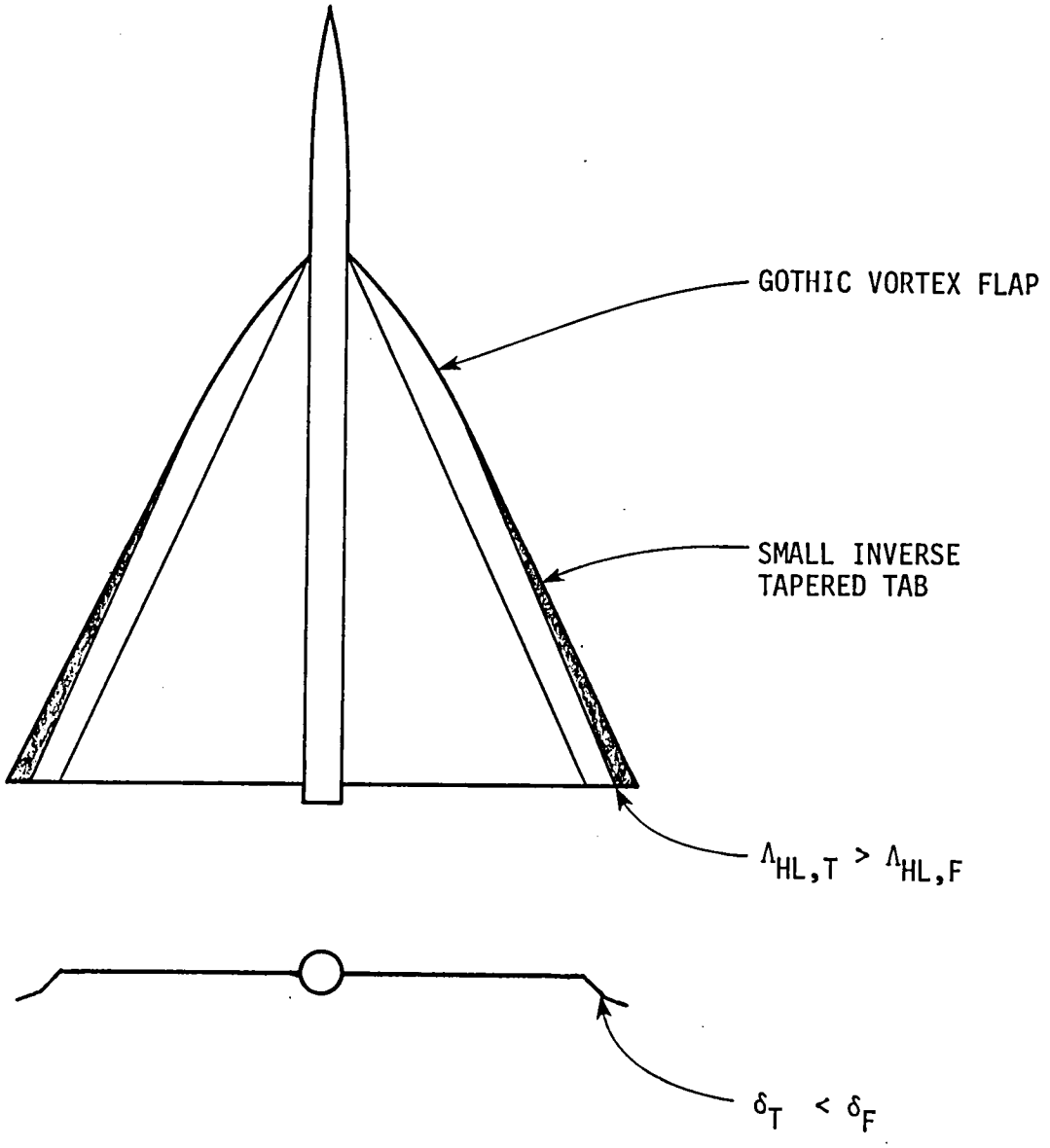

FIG. 30. Suggested vortex flap/tab design features for future investigation.

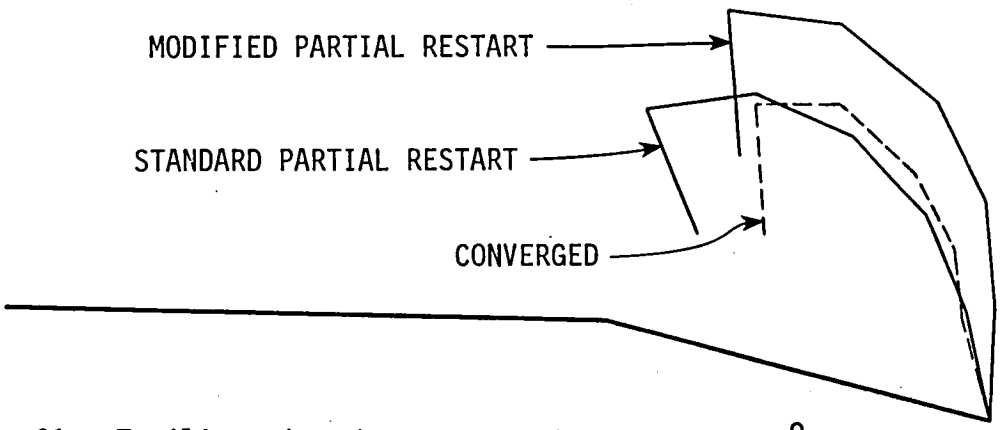

FIG. 31. Trailing edge sheet geometries with $\delta_F = 15^o$ and $\alpha=16^o$, starting solutions taken from planar wing at $\alpha=16^o$ (Modified partial restart: rotation - 15^o, expansion - 5%).

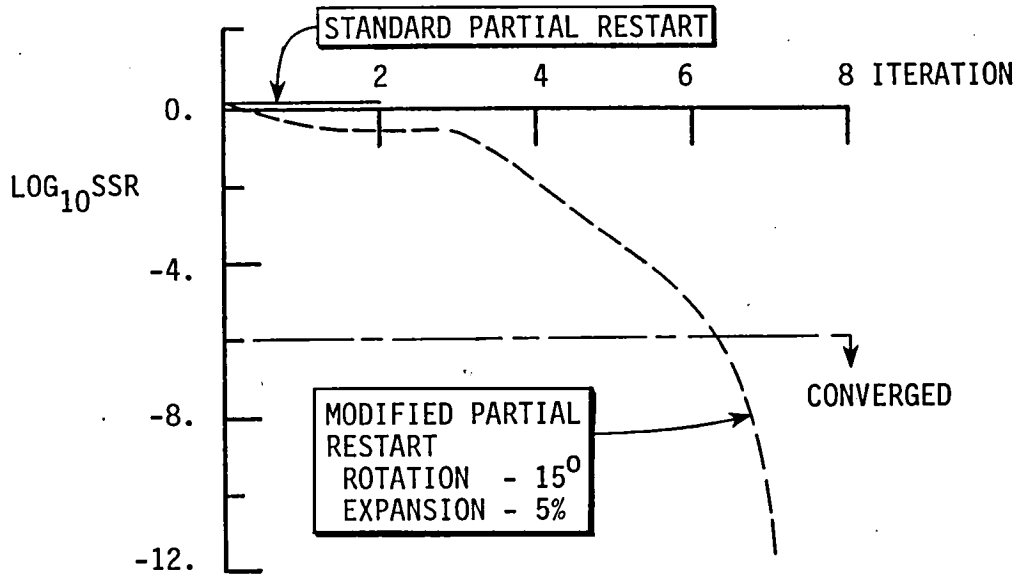

FIG. 32. Convergence rate with $\delta_F=15^o$ and $\alpha=16^o$ using standard and modified partial restart (starting solutions from planar wing at $\alpha=16^o$).

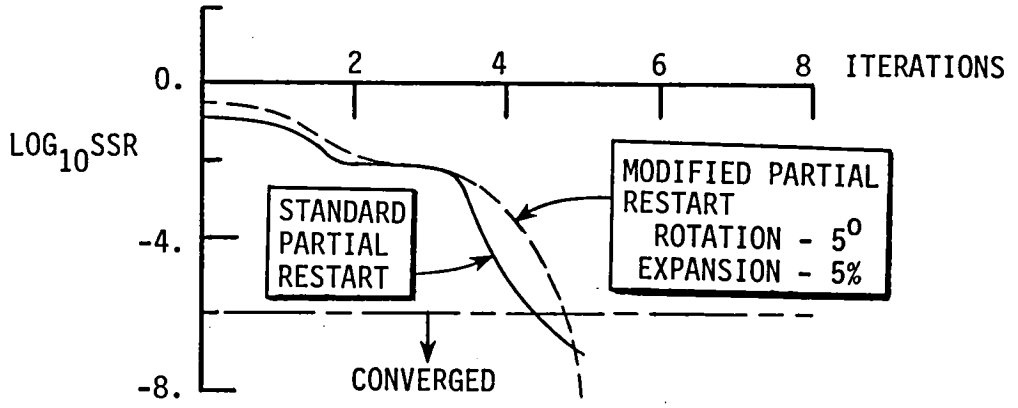

FIG. 33. Convregence rate with $\delta_F=20^o$ and $\alpha=16^o$ using the standard and modified partial restart procedure (starting solutions from $\delta_F= 15^o$ and $\alpha=16^o$).

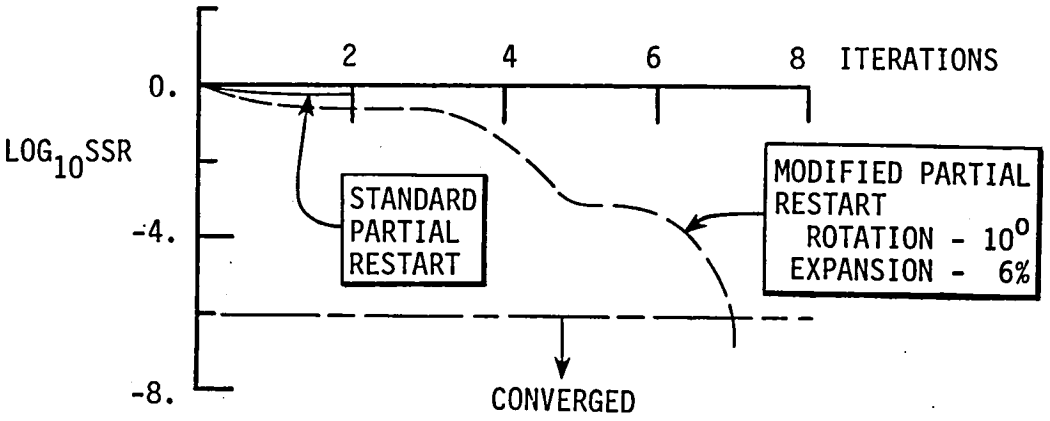

FIG. 34. Convergence rate with $\delta_F=30^o$ and $\alpha=16^o$ using the standard and modified partial restart procedure (starting solutions from $\delta_F=20^o$ and $\alpha=16^o$).

1. Report No.	2. Government Accession No.	3. Recipient's Catalog No.
NASA CR-172586		

4. Title and Subtitle	5. Report Date
Investigation of the "Vortex Tab"	May 1985
	6. Performing Organization Code

7. Author(s)	8. Performing Organization Report No.
Keith D. Hoffler	
	10. Work Unit No.

9. Performing Organization Name and Address	11. Contract or Grant No.
North Carolina State University Department of Mechanical and Aerospace Engineering Raleigh, NC 27695	NCC1-46
	13. Type of Report and Period Covered
12. Sponsoring Agency Name and Address	Contractor Report
National Aeronautics and Space Administration Washington, DC 20546	14. Sponsoring Agency Code 505-31-23-07

15. Supplementary Notes

Published in 1985 as a North Carolina State University Master of Science Thesis.
Langley Technical Monitor: W. Elliott Schoonover, Jr.

16. Abstract

An investigation was made into the drag reduction capability of vortex tabs on delta wing vortex flaps. The vortex tab is an up-deflected leading edge portion of the vortex flap. Tab deflection augments vortex suction on the flap, thus improving its thrust, but the tab itself is drag producing. Whether a net improvement in the drag reduction can be obtained with vortex tabs, in comparison with plane vortex flaps of the same total area, was the objective of this investigation. Wind tunnel tests were conducted on two models, and analytical studies were performed on one of them using a free vortex sheet theory.

The first test was performed on a 65 deg. delta semi-span model with integral conical flap and tab. In this test, upper-surface pressure surveys and flow visualization studies were carried out. The second test consisted of force and upper-surface pressure measurements on a 74 deg. delta wing/body configuration, having constant-chord flaps to which vortex tabs of varied geometry were added. The analytical portion of this investigation employed the Boeing Free Vortex Sheet code to model the 65 deg. delta. Modifications were made to the code to improve its convergence rate.

The vortex tab at relatively small deflection angles improved the lift-to-drag ratio, but reduced it as tab deflection was increased. Tab planform modifications and area reductions were found to improve the lift-to-drag ratio at high vortex flap deflection angles. The free vortex sheet code predicted the correct trends with flap and tab deflections, in both upper surface pressure and vortex core location changes.

The vortex tab was shown to improve lift-to-drag ratio at high lift coefficients. However, it is unclear from this study whether the improvements would outweigh the increased mechanical complexity of the vortex tab.

17. Key Words (Suggested by Author(s))	18. Distribution Statement
Vortex tab Vortex flap Drag reduction Wind tunnel tests Theory	Unclassified - Unlimited Subject Category 02

19. Security Classif. (of this report)	20. Security Classif. (of this page)	21. No. of Pages	22. Price
Unclassified	Unclassified	78	A05